Simulation of the Irradiation Behaviour of the PBMR Fuel in the SAFARI-1 Reactor

B. M. MAKGOPA
20216580

Dissertation submitted in partial fulfillment of the requirements for the degree Master of Science at the Potchefstroom campus of the North-West University

Supervisor: **Mr. T. J. van Rooyen**
Co-supervisor: **Mr. M. Belal**

May 2009

ABSTRACT

Irradiation experiments for the pebble bed modular reactor PBMR fuel (coated fuel particles and pebble fuel) are planned at the South African First Atomic Reactor Installation (SAFARI-1). The experiments are conducted to investigate the behavior of the fuel under normal operating and accelerated/accident simulating conditions because the safe operation of the reactor relies on the integrity of the fuel for retention of radioactivity.

For fuel irradiation experiments, the accurate knowledge and analysis of the neutron spectrum of the irradiation facility is required. In addition to knowledge of the neutron spectrum in the irradiation facility, power distributions and knowledge of nuclear heating values has to be acquired. The SAFARI-1 reactor boosts operating fluid temperatures of about 300 K. On the contrary, the PBMR can reach temperatures in up to about 1370 K under normal operating conditions. This calls for design of high temperature irradiation rigs for irradiation of the PBMR fuel in the SAFARI-1 reactor. The design of this instrument (rig) should be such that to create an isolated high temperature environment in the SAFARI-1 reactor, to achieve the requirements of the PBMR fuel irradiation program. The design of the irradiation rig is planned such that the rig should fit in the existing irradiation channels of the SAFARI-1 reactor, a time and cost saving from the licensing perspective.

This study aims to establish the know-how of coated particle and pebble modeling in using the Monte Carlo N-Particle code (MCNP5). The study also aims to establish the know-how of rig design. In this study, the Necsa in-house code Overall System for the Calculation of Reactors (OSCAR-3), a software known as OScar 3-Mcnp INTerface (OSMINT) linking OSCAR-3 and MCNP5, also developed at Necsa, as well as MCNP5 code developed and maintained by the Los Alamos team, are used to calculate neutronic and power distribution parameters that are important for fuel irradiations and for rig design. This study presents results and data that can be used to make improvements in the design of the rig or to confirm if the required operational conditions can be met with the current preliminary rig design. Result of the neutronic analysis are presented for the SAFARI-1 core, core irradiation channel B6 (where the PBMR fuel irradiation rig is loaded for the purpose of this study), the rig structure and the pebble fuel are presented. Furthermore results of the power distribution and nuclear heating values in the reactor core, the irradiation channel B6, the rig structures and the pebble fuel is also presented.

The loading of the PBMR fuel irradiation rig in core position B6 reduces the core reactivity due to the fact that the loading of the rig displaces the water moderator in channel B6 introducing vast amounts of helium. This impacts on the k_{eff} value because there will be less neutron thermalization and reproduction due to the decreased population of thermal neutrons. The rig is found to introduce a negative reactivity insertion of 46 pcm. The loading of this rig in the core leads to no significant perturbations on the core power distribution. The core hottest channel is still localized in core channel C6 both with RIG IN and

RIG OUT cases. A power tilt is observed, with the south side of the core experiencing reduced assembly averaged fission power, with correspondingly small compensations from the assemblies on the north side of the core.

The perturbations on the core assembly averaged fluxes are more pronounced in the eight assemblies surrounding B6. Core position B6 suffers an 18% neutron flux depression with the loading of the rig. The fluxes in core positions A5, A6, A7, B5, B7 and C7 are increased when the rig is loading. The largest increases are noted as 12% in A7, 9% in A6 and 6% in A5 and B7. All the eight core positions surrounding B6 experience reduced photon fluxes with the loading of the rig. Core position B6 shows a flux depression of up to 20%, with 10% reduction in core position A6. The remainder seven positions surrounding B6 shows flux depressions of no more than 5%.

Further on, due to decreased moderation effects, the axial neutron flux in core position B6 is reduced by 20% when the rig is loaded. The energy dependent neutron flux in B6 decreases by 50% in the thermal energy range with corresponding increases of up to 50% in the resonance and fast energy regions. The axial and the energy dependent photon flux in core position B6 decreases by up to 20% when the rig is loaded.

The magnitude of the neutron and photon fluxes is found to have a direct proportion on the neutron and photon heating values. While the amount of neutron heating in core position B6 increases by one order of magnitude, when the rig is loaded, the photon heating values increases by up to 60% in the region spanning ±10cm about the core centerline. The amount of photon heating in the rig structural materials dominates neutron heating, except in the helium regions of the rig, where neutron heating dominates photon heating. In the fuel region of the pebble, fission heating (3803W) largely dominates photon heating (119W).

Key words: MCNP5, neutron flux, neutron heating, OSCAR-3, pebble, PBMR, photon flux, photon heating, power distribution, SAFARI-1

DEDICATION

To my late father, Moses Makgopa and my mother, Josephine Makgopa.

"For nothing but proper, moral, dignified and principled upbringing"

ACKNOWLEDGEMENTS

This work would not be possible without the grace of the Living God. I bow my head to thank HIM for the wisdom HE bestowed upon me. HE kept me going when I wanted to give up; HE showed me HIS goodness, directed and strengthened me.

Sincere gratitude to Dr. Andy Graham, my former supervisor, for the endless discussions we had surrounding this research study. I also appreciate his contribution in terms of providing OSCAR-3 core exposure and configuration files that made this study possible.

I would like to express sincere gratitude to my dissertation supervisor, Mr. Johann van Rooyen, for giving his time and great efforts during the supervision of this work. The writing of this dissertation was a success given his prompt feedback and comments. His technical and highly professional skills are appreciated and made this work a success.

The patience, dedication and guidance of my co-supervisor, Mr. Mohammed Belal cannot go without being recognized. For his endless support and efforts, helping me to understand and master the fundamental and underlying concepts of the Monte Carlo code system. His efforts and mentorship constitute an invaluable gift.

To my colleagues at Necsa, many thanks to Mr. Lesego Moloko, we spend many hours brainstorming on concepts and approaches to this research work. When the research scope widened and it was hard to determine where to cut-off, Mr. Rian Prinsloo and Dr Gawie Notnagel stepped in for many informal valuable discussions, many thanks to them.

To my kids, Johannes and Leonard, my mother, my siblings “Dinoko”, times were hard during the completion of my course work and this dissertation. I would sometimes go without noticing their presence, when their presence actually motivated me to keep going since it will be a role to them. I cannot go without expressing my deepest gratitude to Mr. Sfako Mehlape, my time companion, for his undivided support, for believing in me, thanks “Kolobe” that kept me going.

PUBLICATIONS

Two papers stemmed out of this research work: The first paper, peer reviewed, was presented at the High Temperature Reactor (HTR2008) conference. The second paper presented at the South African Institute of Physics conference, awarded best M.Sc. oral presentation in the category Applied and Industrial Physics.

i) **B. M. Makgopa**, M. Belal, W. J. Strydom. **Neutronic Characterization of the SAFARI-1 Material Testing Reactor**. Proceedings of the 4th International Topical Meeting on High Temperature Reactors, 28 September-01 October 2008, Washington, D.C, USA

ii) **B. M. Makgopa**, M. Belal, W. J. Strydom. **Characterization of the SAFARI-1 Material Testing Reactor**. 53rd Annual Conference of the South African Institute of Physics, 8-11 July 2008, University of Limpopo, South Africa.

TABLE OF CONTENTS

TABLE OF CONTENTS (continued)

LIST OF FIGURES

LIST OF FIGURES (continued)

LIST OF TABLES

LIST of ACRONYMS and ABBREVIATIONS

AGR	Advanced Gas Reactor
ATR	Advanced Test Reactor
AVR	ArbeitsgemeinschaftVersuchReaktor
BISO	A double layer composed of pyrolytic carbon
BoC	Beginning of Cycle
BoL	Beginning of Life
BTE	Boltzmann Transport Equation
CFP	Coated Fuel Particle
CORANA	CORe ANAlysis
CROGEN	CROss section GENerator
CROLIN	CROss section LINker
EFPD	Effective Full Power Days
ENDF	Evaluated Nuclear Data File
ENDL	Evaluated Nuclear Data Library
ESKOM	Electricity Supply COMmission
FIMA	Fissions per Initial Metal Atom
GT	Gas Turbine
GT-MHR	Gas Turbine Modular Helium Reactor
HEU	High Enrichment Uranium
HFIR	High Flux Isotope Reactor
HFR	High Flux Reactor
HP	High Pressure
HPT	High Pressure Turbine
HTGCR	High Temperature Gas Cooled Reactor
HTR	High Temperature Reactor
HTTR	High Temperature Test Reactor
INEEL	Idaho National Engineering and Environmental Laboratory
INET	Institute of Nuclear Energy and Technology
JAERI	Japan Atomic Energy Research Institute
JRC	Julich Research Center
LANL	Los Alamos National Laboratory
LEU	Low Enrichment Uranium
LOCA	Loss Of Coolant Accident
LP	Low Pressure
LPT	Low Pressure Turbine
HTGCR	High Temperature Gas Cooled Reactor

LIST of ACRONYMS and ABBREVIATIONS (continued)

HTR	High Temperature Reactor
IPyC	Inner Pyrolytic Carbon
MC	Monte Carlo
MCNP	Monte Carlo N-Particle
MeV	Mega electron Volts
MEDUL	MEhrfach DUrchLauf (multipass refueling)
MGRAC	Multi Group AnalytiC nodal diffusion code
MTR	Material Testing Reactor
MONTEBURN	MONTE Carlo BURN-up code
MWd/tU	MegaWatt Days per Ton of uranium
MW(e)	MegaWatt Electric
MW(th)	MegaWatt Thermal
NECSA	South African Nuclear Energy Corporation
OPyC	Outer Pyrolytic Carbon
ORNL	Oak Ridge National Laboratory
OSCAR	Overall System for CAlculation of Reactors
OSMINT	OScar-3 Mcnp INTerface
PBMR	Pebble Bed Modular Reactor
PCU	Power Conversion Unit
PIE	Post Irradiation Examination
RPV	Reactor Pressure Vessel
SAFARI	South African First Atomic Reactor Installation
THTR	Thorium High Temperature Reactor
TRISO	TRIpple ISOtropic , four layers (buffer/IPyC/SiC/OPyC)
TRIZO	TRIpple IZOtropic (IPyC/ZrC/OPyC) – with ZrC replacing SiC of TRISO
UK	United Kingdom
U.S.A	United States of America
VHTR	Very High Temperature Reactor

NOMENCLATURE

Ag	Silver
B_4C	Boron Carbide
UC_2	Uranium Carbide
CO	Carbon Monoxide
UCO	Uranium Carboxyl
UO_2	Uranium Dioxide
Pd	Palladium
PuO_2	Plutonium Dioxide
SiC	Silicon Carbide
SS316	Stainless Steel 316
ThO_2	Thorium Dioxide
ZrC	Zirconium Carbide

CHAPTER I: BACKGROUND ON THE PBMR

I.1 INTRODUCTION

The pebble bed modular reactor (PBMR) is a high temperature gas cooled reactor (HTGCR) new to the nuclear history of South Africa. The PBMR initiative is led by ESKOM with the demonstration reactor to be constructed on the Koeberg site in the Western Cape. This technology builds on the operational experience of the German reactors: AVR and HTR-Modul, the United States experience with Peach Bottom I and Fort St. Vrain and Britain's Dragon reactor [1]-[3]. Due to increasing electricity demands in South Africa, with coal power stations reaching their end of life and concerns about global warming, it is necessary for the country to start exploiting the uranium resources.

This chapter gives an overview of the PBMR in section I.2. The problem statement is presented in section I.3. Research tools and objectives are discussed in section I.4 and I.5 respectively and lastly the outline of the rest of the thesis is given in section I.6.

I.2 THE PBMR

The PBMR derives its name from the type of fuel it uses ("pebbles") and the modular fashion in which it is constructed. It is a small unit reactor, the size of which can be adjusted according to the community or industrial need, and is ideal for location at remote sites. The reactor operates on a direct, closed Brayton cycle with recuperation to convert the heat, which is generated in the core by nuclear fission and transferred to the coolant gas, and into electrical energy by means of a gas turbo-generator [1]-[3]. A single 400 MW (th) module of the PBMR is expected to generate a total of about 165 MW (e) with an efficiency of about 41% [2], [3].

The key design characteristics of the PBMR are the use of graphite as a moderator, helium as a coolant and the TRIple ISOtropic (TRISO) -coated ceramic fuel. The TRISO fuel acts as a fission product retention barrier during normal operations as well as under accident conditions [1]-[3]. The advantages to using helium as a coolant is that it remain single phase under all conditions and it is invisible to the neutrons (i.e. it does not affect the neutron behavior-neutronically inert). The advantage to using a graphite moderator is that it has a high heat capacity; hence it remains stable at very high temperatures. It also has low neutron capture cross section because the carbon-12 nucleus is highly stable.

I.2.1 Physical Description of the PBMR

The module components are contained within four steel pressure vessels: the reactor system vessel, two turbo compressor units and the power generation turbine. For improved thermodynamic efficiency recuperation and inter-cooling of the helium coolant gas is allowed [1]. The power conversion unit (PCU)

in *Figure I.1* consists of the compressors and turbines, gearbox, power generator, recuperator, precooler and intercooler [1]. The latter three components are there to boost the efficiency of the plant. The main function of the PCU is to convert heat received from the reactor into electrical energy.

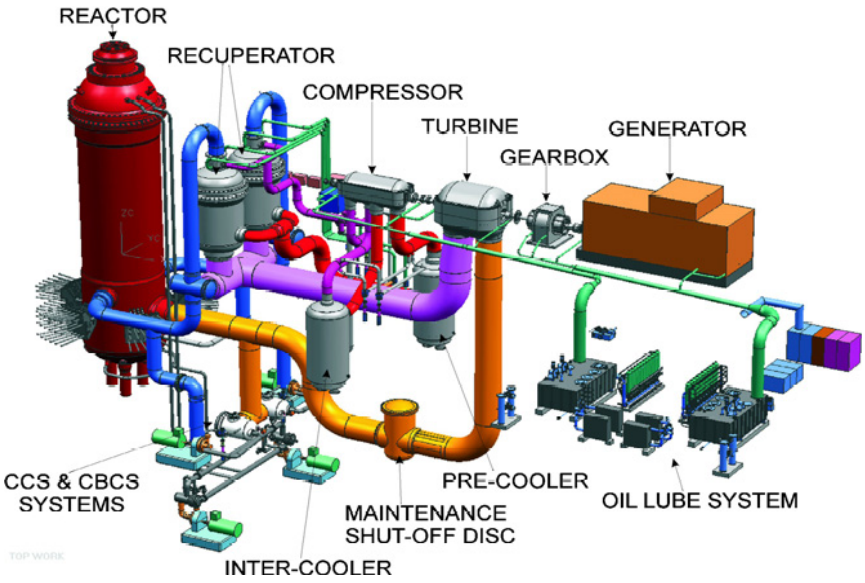

Figure I.1: Physical Layout of the PBMR Power Conversion Unit [4].

Figure I.2 represents a Brayton cycle with recuperation and inter-cooling and it is explained briefly in terms of the helium coolant flow. The coolant leaves the core at 900˚C and enters the high pressure turbine, transferring some energy to drive the electric generator and the compressor. Helium then enters the low pressure side of the recuperator and then proceeds to the precooler. Helium flows through to the compressor to the intercooler, then to the high pressure compressor into the high pressure side of the recuperator before entering the core at about 500˚C.

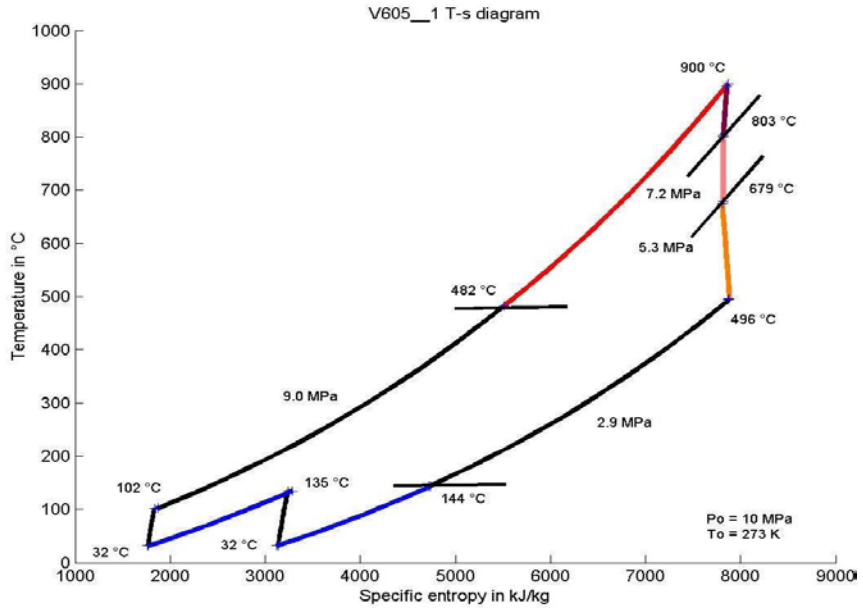

Figure I.2 : A Temperature-Entropy (T-S) Diagram of the PBMR Brayton Cycle ***[6]***

I.2.2 PBMR Core Design

The PBMR consists of a vertical steel Reactor Pressure Vessel (RPV) with an inner diameter of 6.2 meters and a height of about 27 meters [4]. The RPV contains a core barrel which supports the annular core of an inner diameter of 2 meters (fixed central reflector), an outer diameter of 3.7 meters (pebble channel) and an effective core height of 11 meters. The annular reactor core structure has got comprise a fixed central reflector with an inner diameter of 2.0 meters and an outer diameter of 3.7 meters. The active core contains approximately 452 000 fuel spheres packed in the region indicated in *Figure I.3* as the Pebble Channel. The Reactivity Control System (RCS) consists of 24 control rods in the side reflector region. These rods contain B_4C, a neutron absorber. The Reserve Shutdown System (RSS) is capable of inserting small graphite spheres containing the B_4C absorber into the channels in the fixed central reflector-for reactivity control [5].

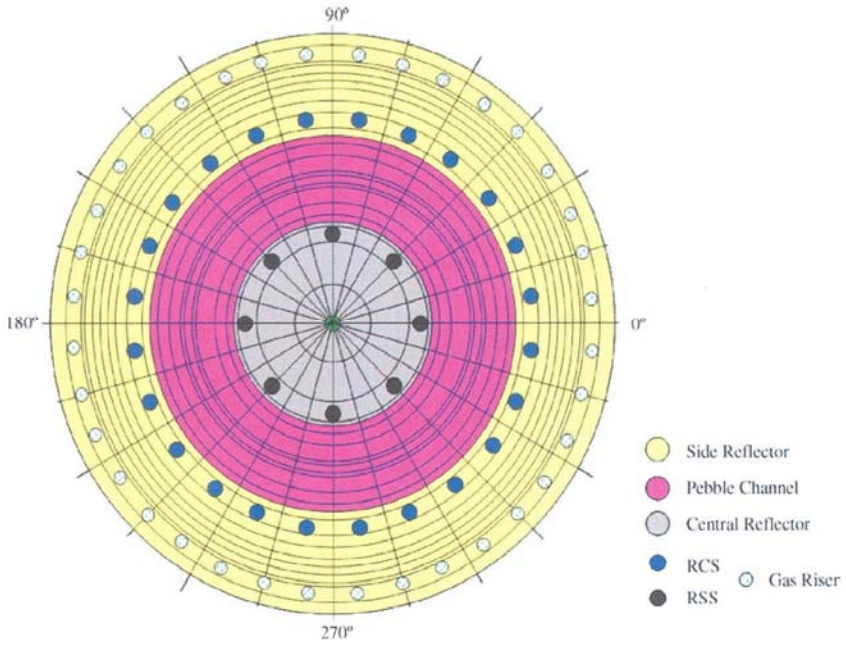

Figure I.3: Cross sectional view of the PBMR pressure vessel [4]

An annular core is adopted and ensures low power densities and this ensures that the fuel temperatures remain well below the maximum temperatures that can challenge the integrity of the fuel even in the case of loss of coolant accidents (LOCAs). The long annular core results in a relatively low power density of about 4.8 MW(th)/m^3, which is an important passive safety feature.

The PBMR also operates on a MEDUL refueling concept. This is an online refueling mechanism with multiple passes through the core. Pebbles are fed at the top of the core and removed at the bottom. As they exit the core, their mechanical integrity is assessed and their burn-up is measured. If a fuel sphere has reached the target burn-up and/or its mechanical integrity is compromised it will be removed from the system, otherwise it will recirculate into the core.

I.3 THE PBMR FUEL

The PBMR fuel fabrication plant is housed at Pelindaba. The PBMR fuel is manufactured with the objective to be equivalent to the German high temperature reactor (HTR) fuel, with equivalence defined as using the same process as was used in the German program, using the same materials, using the same fuel design and using the same quality assurance methodology [8].

I.3.1 TRISO Coated Fuel Particles

The coated fuel particle (CFP) consists of spherical redundant layers which are designed in such a way that they retain the fission products. The TRISO particles have four coating layers which encapsulate the fuel kernel, a dense microsphere which contains the fissile material. Each layer serves a specific purpose but the overall purpose is to act as a high integrity pressure vessel for fission product retention. The dimensions and material composition of the fuel are summarized in *Table I.1*.

Table I.1: Material Properties and Dimensions of the PBMR Fuel [9]

Property	Value
Enrichment	9.8 weight percent ^{235}U
U mass per kernel	0.62 mg
Materials	
Kernel	Uranium oxide (UO_2)
Inner Pyrolytic (IPyC) layer	High density pyrolytic carbon
SiC layer	SiC
Outer Pyrolytic (OPyC) layer	High-density pyrolytic carbon
Dimensions (μm)	
Kernel diameter	500
Buffer layer thickness	93
IPyC layer thickness	38
SiC layer thickness	35
OPyC layer thickness	40
Material densities ($g.cm^{-3}$)	
Kernel	10.8
Buffer layer	1.01
IPyC layer	1.86
SiC layer	3.19
OPyC layer	1.89

The uranium dioxide (UO_2) fuel kernel has a maximum theoretical density of 10.96 g/cm^3. In the case of the PBMR fuel, the density is allowed to vary from about 10.5 g/cm^3 to 10.8 g/cm^3. The fissile UO_2 is contained in a 0.025 cm radius region. The main function of the kernel is to produce fission power. The carbon buffer layer surrounds the kernel, with a layer thickness of 93 μm and a density of 1.01 g/cm^3. The buffer layer serves as a reservoir for fission gases released from the kernel and to attenuate fission recoils.

The buffer layer is surrounded by the inner pyrolytic carbon (IPyC) layer of thickness 38 μm and a density of 1.86 g/cm^3. The IPyC serves as a smooth substrate for deposition of a high quality silicon carbide layer and to prevent chlorine and hydrochloric acid from entering the fuel kernel during the deposition process. The silicon carbide (SiC) layer surrounds the IPyC layer with a layer thickness of 35 μm and a density of 3.19 g/cm^3. The SiC layer provides structural strength and dimensional stability and also serves as a barrier for fission product retention, particularly the metallic products. Finally the SiC layer is surrounded by the outer pyrolytic carbon (OPyC) layer of thickness 40 μm and a density of 1.89 g/cm^3. The OPyC layer provides a smooth bonding for the production of fuel pebbles.

I.3.2 The Pebble Fuel

In manufacturing the pebble, a mixture of about 15 000 TRISO coated particles is embedded in a graphite matrix, cold pressed into a spherical fuel region of 50 mm in diameter and then cold presses again within an envelope of pure graphite matrix to yield a final fuel sphere or pebble of 60 mm in diameter [1]. The schematic of the TRISO CFP and the pebble fuel is given in *Figure I.4* below.

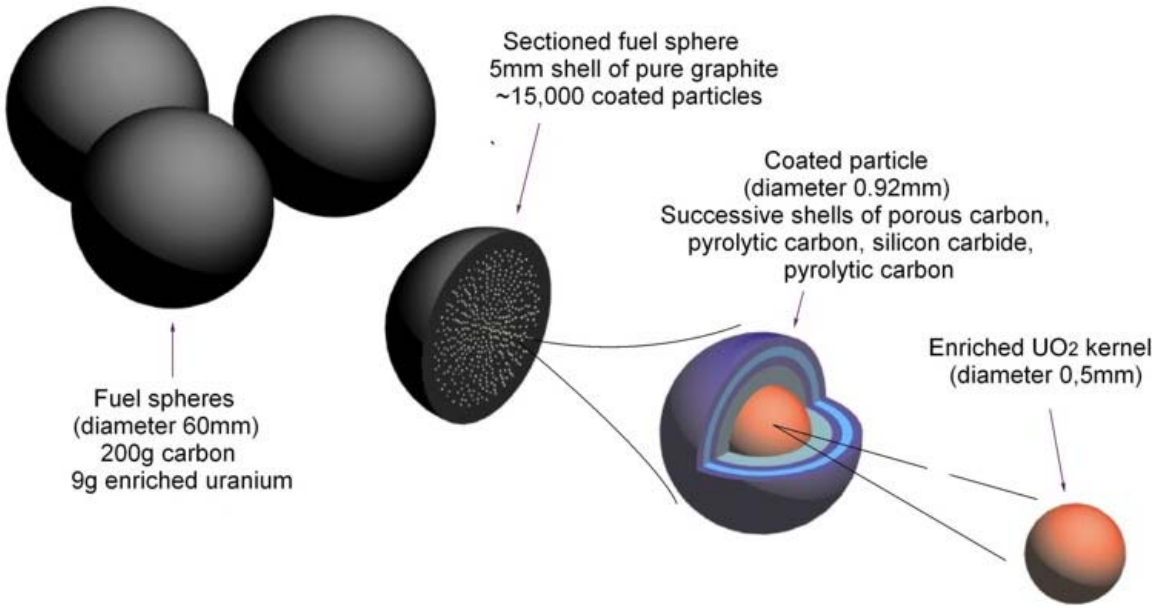

Figure I.4: The PBMR pebble fuel and TRISO coated fuel particles (CFP) [7]

I.4 FUEL PERFORMANCE AND FAILURE MECHANISMS

This subsection presents different failure mechanism for the HTR fuel. The failure of the fuel can be seen as due to the as-manufactured defects and operational defects. Fuel failure is of statistical nature since not all of the particles will fail at the same time, but only a fraction will, when some parameters are exceeded. Failure of the fuel particles is strongly dependent on the fast neutron flux, temperature and burn-up which are the parameters that span the scope of this research.

I.4.1 As-Manufactured Defects

This category includes failure of particles following the pressure vessel failure mode due to defective or missing coatings. Irradiation induced failure of the IPyC and OPyC with potential cracking of SiC also falls under this category [10].

I.4.2 Operational Defects

Failure of the fuel due to operational effects is classified into four categories. Each of these categories is explained below.

I.4.2.1 Pressure Vessel Failure

This is of more concern at high fuel burn up. The accumulation of gaseous fission products leads to a pressure build-up inside the fuel. During irradiation the IPyC and the OPyC layers undergo shrinkage and creep. The pyrolytic carbon layers are, as a result, put into tension and also apply a compressive force on the elastic SiC layer. This pressure exerts a tensile stress on the coated layers. If this tensile stress exceeds the strength of the layers, then the fuel will fail [10].

I.4.2.2 Kernel Migration

This failure mechanism is also referred to as the "*amoeba effect*". This effect has a strong dependence on temperature. As the temperature gradients across a coated fuel particle increases, the kernel will tend to migrate towards the high temperature side (i.e. up along the thermal gradient) [10].

I.4.2.3 Chemical Attack of the Sic Layer

This mechanism shows a strong dependence on temperature and burn-up. During fission, noble metals (Palladium, Pd and Silver, Ag included) form at high concentrations. Since they cannot form stable metal oxides at such operating conditions, they tend to migrate out of the fuel. Pd normally sits at the inner

surface of the SiC layer but may penetrate this layer at high temperatures and lead to fission product release. Silver diffuses through the intact SiC layer, carries some radioactivity with it and poses maintenance problems [9]. In the UO_2 fuel, oxygen is formed during fission of the heavy metal. At high temperatures this oxygen will react with the carbon in the SiC layer as follows:

$$2C + O_2 \rightarrow 2CO \qquad \text{I-1}$$

As a result, carbon monoxide (CO) will form on the high temperature side and overpressure from this gas can lead to fuel failure [10].

I.5 SAFETY OF THE PBMR

The safety requirements of the PBMR and other high temperature reactors are a combination of passive and inherent mechanisms. The passive requirement is in the high heat capacity of the graphite core. The inherent safety requirement is in the negative temperature coefficient of the fuel, hence the entire core. The following principles of stability adopted in high temperature reactors also apply to the PBMR: nuclear, thermal, chemical and mechanical and are briefly presented below.

I.5.1 Nuclear Stability

Nuclear stability entails that nuclear transients may never lead to unallowable power excursions or overheating of the fuel. The reactor should be designed with mechanisms allowing for self-acting limitation on nuclear power. This stability is ensured by the large negative feedback coefficient of the fuel. This together with the void coefficient of the He moderator yields a large negative temperature feedback coefficient. The continuous (online) loading and unloading of pebbles in the core ensures that very small excess reactivity is needed to compensate for burn-up and the fuel is stable up to very high temperatures [11]

I.5.2 Thermal Stability

Thermal stability of the core implies that the core may never melt or overheat. The reactor is then designed with self-acting decay heat removal mechanisms to ensure this. The mechanisms are: (1) retention of fission products in the fuel up to high temperatures, (2) the use of ceramic material which ensures a temperature resistant core, (3) the high heat capacity of graphite also ensures that the core heats up slowly, (4) the low core power density allows for passive heat removal, (5) effective heat removal by natural processes (conduction, radiation and free convection) even during loss of coolant, with the environment acting as a large and permanent heat sink [11].

I.5.3 Chemical Stability

Chemical stability of the core implies the self-acting integrity of the core against corrosive attack. This is achieved through the use of the inert helium coolant which will not undergo any chemical reaction with the fuel and core components. The coolant is transparent to neutrons. The coolant also remains single-phase under all conditions, so that bulk boiling is avoided. A leak tight hence burst-proof prestressed concrete reactor building (containment/confinement) puts limitation on air and water ingress, so that the reaction between graphite and air (or water) is avoided. The ceramic fuel elements are non-corrosive and ensure a temperature resistant core. The effective heat removal by natural processes (conduction, radiation and free convection) even during loss of coolant and the environment acts as a large and permanent heat sink [11].

I.5.4 Mechanical Stability

The mechanical stability of the core and the fuel implies the self acting integrity of the core against mechanical failure. The SiC layer of the fuel has a large heat resistance. This together with the other layers ensures the stability of the fuel against mechanical failure. Fission products can only be released if all the layers fail and maybe the pressure vessel as well. In addition to the multiple containment layers (in the fuel) and the steel pressure vessel, the graphite core and the reinforced concrete reactor building structure also ensure a fail-safe reactor [11].

I.6 PROBLEM STATEMENT

Fuel for the PBMR is fabricated at the South African Nuclear Energy Corporation (Necsa) using a sol-gel (external gelation) process to produce the UO_2 kernels, followed by a step-wise precipitation of coating layers using chemical vapour deposition [46]. Quality control measures are taken at each manufacturing step, amongst others: x-ray studies (radiography) to determine the thickness of layers and detect missing layers, burn and leach methods to detect defective SiC layers and tests to determine the sphericity of the fuel particles [10].

During irradiation, the fuel undergoes changes in chemical composition and physical properties. The probability of failure of coated particles thus depends on the relative magnitude of the flux in the different regions of the neutron spectrum more especially the fast neutron flux. Particle failure is also dependent on fuel temperature and the degree of burn-up. The knowledge of the thermal spectrum in the fuel zone is very important since it determines the burn-up of U-235 in the fuel. The knowledge of the fast neutron flux spectrum is also important as it is the primary cause of damage to the SiC layer.

Fuel irradiation experiments are to be conducted on the Necsa fabricated fuel at the South African First Atomic Reactor Installation (SAFARI-1 reactor). The purpose of these experiments will be to qualify the

fuel for high temperature applications and determine if it meets the design specifications. The experiments will support the licensing of the fuel manufacturing process and the licensing of the fuel for use in the PBMR. Experimental results will aid to benchmark fission gas release and fuel performance models and assist with the verification and validation of code system used in calculations. Irradiated fuel will also be available for post irradiation examination (PIE).

A preliminary rig or capsule has been designed to contain the pebble fuel for insertion in the reactor during irradiation testing. Fuel irradiation in the SAFARI-1 material testing reactor (MTR) has to take place under conditions that simulate the high temperature operating conditions in the PBMR. This requirement is achieved through rig design. A rig is designed such that a pebble fuel inserted in graphite is contained in a capsule. This capsule, cooled by inert helium (stagnant or flowing) is then inserted into a rig that is cooled on the inside by another helium gas loop and on the outside by the reactor water coolant. Adjusting the size of the gas gaps has an effect on the spatial temperature distribution in the rig.

It can be very costly for such a rig to be designed and manufactured with instrumentation (fission gas monitors and high temperature thermocouples) prior to doing theoretical (code) calculations of the neutronics and thermal hydraulics of the rig and the pebble fuel. Such calculations need to be done to determine the radial and axial neutron and photon flux spectrum (thermal and fast) together with the heating rates in all the regions of the fuel and the rig. The results of these will be feedback into thermal hydraulic codes to determine temperature distributions, thereby confirming that the rig design will simulate the desired high temperature environment.

The planned PBMR fuel irradiation experiments might impact on the core neutronic characteristics and irradiation capabilities. The loading of this rig in core position B6, might impact on:

- Reactivity of the core
- Core neutron and photon flux spectrum
- Core power distribution
- Neutron flux spectrum in the core irradiation positions hence affecting the planning in terms of irradiation of other materials and isotope production.

I.7 RESEARCH TOOLS

Necsa has a number of software tools to its disposal to study irradiation conditions inside SAFARI-1. These are:

- A reactor core analysis code package known as **O**verall **S**ystem for **CA**lculation of **R**eactors (OSCAR) that is used to perform core follow calculations for SAFARI-1 and produces a quasi static time-dependant isotopic distribution of selected materials throughout the reactor core. It

utilizes diffusion theory which is not adequate for detailed evaluation of strongly anisotropic flux behaviour, as is found in the core periphery where some irradiation positions are situated [12]. In late 2007, there was a transition from OSCAR-3 to OSCAR-4, the new version that will include a detailed core thermal hydraulic model. The calculations in this work are performed using OSCAR-3.

- Monte Carlo N-Particle (MCNP) code that can be used to perform detailed transport calculations to determine exact neutron flux behaviour in high energy and spatial detail, but requires an isotopic material distribution as input [13]. For the purpose of calculations in this work, the code MCNP5 version 1.4 is used.

- OScar-MCNP INTerface (OSMINT), which is an existing software tool to couple OSCAR-3 and MCNP, such that the required OSCAR-3 isotopic data for selected isotopes are passed to a MCNP model of the reactor, hence setting up an MCNP input file which is accurate in time and space [14].

The three tools can be used in conjunction to study the irradiation conditions prevalent inside the fuel pebble(s) in the rig, inserted in a particular irradiation position inside SAFARI-1. The following approximations are inherent in this approach, and therefore a certain amount of discrepancy between OSCAR, MCNP and experiment is expected because:

- ✓ MCNP stochastically solves the neutron transport problem utilizing its own continuous energy cross section library [13], while OSCAR-3 solves the core neutronics problem deterministically via diffusion theory, based on a 172 groups WIMS library [12].
- ✓ Only a defined number of isotopes (39 at this point) are transferred from OSCAR-3 to MCNP, and the remaining fission products are considered neutronically unimportant. This assumption needs to be quantified.

I.8 RESEARCH OBJECTIVES

The general aim of this project is to establish an essential part of the know-how to assist with the support of rig design and irradiation of PBMR fuel and entails the use of the three tools mentioned above with emphasis on MCNP simulation of neutronic conditions inside the fuel. The project entails the following:

- Become familiar with the basic physics, assumptions and simplifications inherent in the OSCAR-3 code with emphasis on how that may influence the final MCNP results.
- Assist with the testing and verification of the OSMINT to ensure that OSCAR-3 material and geometric data is correctly transferred to the MCNP model of SAFARI-1.

- Understand the physics underlying the link; explore the advantages and disadvantages of the link.
- Accurate modeling of the coated fuel particle (produce an explicit heterogeneous model including the kernel and all the coating layers) and the pebble as well as modeling of the irradiation rig with the pebble inside.
- Generate a geometrical model of the SAFARI-1 core using OSMINT, with the whole core material composition accurate in space and time (i.e. representative of the OSCAR core follow of a specific day and time).
- Utilize the MCNP model of the SAFARI-1, include a model of a standard rig and fuel pebble in the desired irradiation position and calculate the neutron spectrum, fission heating terms, gamma heating terms and characterize the degree of isotropy of the neutron flux.

The results of the final calculations, that will span a range of parameters applicable to fuel irradiation, will be essential for proper fuel rig design and irradiation of the fuel under pre-set neutron flux and temperature conditions.

I.9 LAYOUT OF THE DISSERTATION

Chapter I present a description of the PBMR: physical description, core design and fuel design. In this chapter, fuel performance and failure mechanisms together with the safety features of the PBMR are also presented. The last sections of this chapter include the problem statement, the research tools and the research objectives

In Chapter II, a description of the past and recent developments in high temperature technology is given. This starts with a brief background on fuel evolution followed by a description of different types of high temperature reactors. The HTR materials and fuel irradiation facilities together with the fuel irradiation experiments are also presented in this chapter.

Chapter III presents the neutron transport equation, as a fundamental equation governing the spatial, time and angular dependent neutron population. The rest of the chapter focus on describing the three code systems (OSCAR-3 and OSCAR-3, MCNP and OSMINT) that will be used in this work and their limitations, advantages and disadvantages.

Chapter IV presents simulation and geometrical models for the coated fuel particle, pebble fuel, irradiation rig and the SAFARI-1 reactor. A discussion of the parameters that will be investigated in this study is also presented in this chapter. Result and discussions are presented in Chapter V. Finally conclusions and recommendations for future work are presented in Chapter VI and Chapter VII respectively.

CHAPTER II : HISTORY OF HIGH TEMPERATURE REACTORS

II.1 INTRODUCTION

This chapter gives an overview of the historical and recent developments of high temperature reactors. An overview of the high temperature (HTR) fuel irradiation facilities as well as the HTR fuel irradiation experiments is also presented. Section II.2 gives an overview of the different fuel design used in high temperature reactors and provides a brief background on the fuel evolution. Section II.3 gives a brief description of the HTR reactors, old and new developments. Facilities that were used for HTR fuel irradiation together with those are still in use are presented in section II.4 with information on the different HTR fuel irradiation experiments conducted.

II.2 EVOLUTION OF THE HTR FUEL

The early designs of the HTR fuel were only made of two layers (BISO) surrounding surrounding the kernel. These were the buffer and two pyrolytic layers only. A variety of kernel compositions including uranium/thorium carbide $(U/Th)C_2$, uranium carboxyl (UCO), plutonium oxide (PuO_2) and uranium/thorium oxide $(U/Th)O_2$ were manufactured and used in high temperature reactors. Various dimensions of the kernel and coating layers were also investigated. The integrity of this fuel proved very poor during a series of fuel irradiation experiments in the United States of America (U.S.A) and Germany. Also designs moved from high enriched (93%) to low enriched fuel (less than 20%) [10], [15].

This prompted research into alternative fuel designs. In moving away from the BISO fuel, a third coating layers was introduced, the silicon carbide (SiC) layer to make a so-called “TRISO” coated fuel particle. The description of the TRISO fuel is given in chapter I. In a series of irradiation experiments, the German made fuel proved to be significantly more reliable than the BISO coated particles, with little amounts fission gases released and very minimal particle failure compared to the U.S.A fuel [10], [15].

Recent research has focused on investigating the possibility of replacing the SiC layer with a zirconium carbide (ZrC) layer to increase the structural or mechanical stability and fission production retention capability of the fuel [10], [15]. This is a move from the TRISO to the TRIZO fuel. The latter is more stable and less susceptible to degradation by palladium attack at high temperatures. The PuO_2 fuel kernel is preferred to the UO_2 fuel kernel in the Gas Turbine Modular Helium Reactor (GTMHR) concept of Russia.

There are two competitive fuel designs: the German design uses spherical fuel elements embedded in a graphite matrix and the U.S.A fuel is loaded into a graphite hexagonal prism (prismatic fuel elements) including the pin-in block type of Japan [16]. The different fuel designs are shown in *Figure II.1* below:

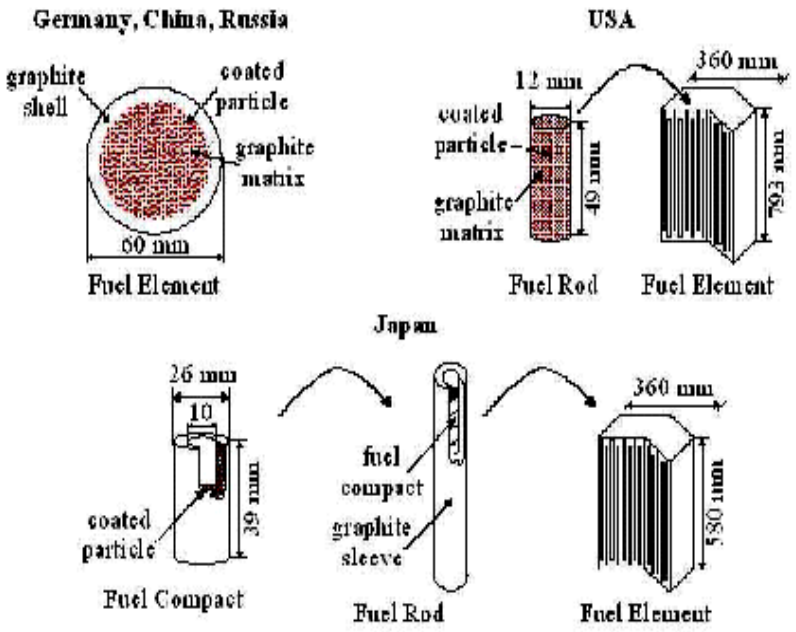

Figure II.1: Fuel Designs for Different Reactor Concepts and Countries [16]

II.3 HIGH TEMPERATURE GAS COOLED REACTORS

This section presents the history of high temperature gas cooled reactors. Only two reactors were built and operated in Germany, the Arbeitsgemeinschaft Versuchreaktor (AVR) and the Thorium High Temperature Reactor (THTR). Many gas cooled reactors, including the Dragon reactor, were built and operated in the United Kingdom (UK). In the United States of America (USA), two reactors were built and operated: the Peach Bottom I and Fort St. Vrain reactors. All these reactors were gas cooled and graphite moderated. The German reactors were employed pebble type fuel, while the U.S.A and U.K designs employed hexagonal fuel assemblies made of fuel compacts and rods. In the next sections, a brief description of each of these reactors is presented. The reactors are divided into two classes: the steel pressure vessel and the pressurized concrete reactor vessel. Only a description of the reactors that were designed, built and operated is presented. Some of the reactors, mostly of German designs: the HTR-500, HTR-100 and HTR-Modul only reached a design stage but were never built and operated. The details of these reactors will not be presented in this literature study. It is very important though to mention that the design of the PBMR is based on the German experience with the design and operation of their HTRs.

Also discussed in this section, is the latest developments in HTR technology. Brief descriptions of the Japanese design of the High Temperature Test Reactor (HTTR) and the Chinese High Temperature Reactor (HTR-10) are presented. Further on, a new design by the U.S.A, the Gas Turbine-Modular Helium Reactor (GT-MHR) and the South African design of the PBMR are presented. All these reactors are described in terms of reactor thermal and electrical power, coolant inlet and outlet temperatures where applicable.

II.3.1 Steel Pressure Vessel Reactors

II.3.1.1 The Dragon Reactor

Figure II.2: The Dragon Reactor [17]

This experimental reactor was built at Winfrith in the UK. The reactor was used as a test-bed for fuels and materials in support of the European HTR technology. It went into operation in 1965 and reached its full capacity, 20 MW (th) in 1966. The graphite cylindrical fuel elements used in this reactor consisted of high enriched uranium-carbide coated particle [19]. The reactor was in operation until shutdown in 1976. The core inlet and outlet coolant (helium) temperatures were 350 °C and 750 °C respectively [21].

II.3.1.2 Peach Bottom 1

Figure II.3: The Peach Bottom-1 Reactor [17]

The first HTR power plant, the Peach Bottom 1, was built in the U.S.A, Philadelphia. The reactor operated at a thermal output power of 110 MW and a gross electrical output power of 40 MW. The reactor reached its first criticality in 1966 and started commercial operation in 1967 [20]. It remained in operation until 1974. The reactor used high enriched uranium and thorium fuel contained in cylindrical fuel elements. The helium coolant inlet and outlet temperatures were 377˚C and 750˚C respectively [21].

II.3.1.3 The Arbeitsgemeinschaft Versuchreaktor (AVR)

Figure II.4: The AVR Building [17]

The AVR is an experimental pebble bed reactor that was built at the Julich Research Center (JRC) in Germany. This 46 MW(th) and 15 MW(e) reactor reached its first criticality in 1966 and it was connected to the electricity supply grid in 1967. The reactor remained in operation until 1988. The reactor employed spherical fuel elements containing the fissile HEU and thorium. The AVR reached a maximum core helium outlet and inlet temperatures of 950˚C and 270˚C respectively [20], [21].

II.3.2 Pressurized Concrete Vessel Reactors

II.3.2.1 Fort St. Vrain

Figure II.5: Fort St.Vrain Reactor [17]

The 842 MW (th) power plant was also built at Colorado in U.S.A. The reactor went into commercial operation with an electrical output power of 330 MW (e) [20]. The reactor used block type fuel elements with a fissile HEU and fertile thorium, uranium/thorium carbide variant. This reactor went critical in 1974 and operated until 1989 when it was decommissioned due to escalating operating costs. The core helium inlet and outlet temperatures have reached 400°C and 775°C respectively [21], [22].

II.3.2.2 Thorium High Temperature Reactor (THTR)

Figure II.6: The THTR Reactor [17]

This 750 MW (th) and 300 MW (e) pebble bed type reactor was built and operated in Germany. The reactor was connected to an electrical grid in 1985 it remained in operation until shut down in 1989 [19]. The coated fuel particles were manufactured of (Th/U)O_2 high enrichment kernels of the BISO type. The core helium inlet and outlet temperatures reached 250 °C and 750 °C respectively [23].

II.4 RECENT DEVELOPMENTS IN HTR TECHNOLOGY

II.4.1 High Temperature Test Reactor (HTTR)

Figure II.7: The HTTR [18]

The first high temperature reactor by JAERI (Japan Atomic Energy Research Institute) achieved its first criticality in November 1998. The reactor is graphite moderated; helium gas cooled and has a maximum power output of 30 MW. The maximum coolant outlet temperature is 950°C with an inlet temperature of 395°C [5]. The reactor uses low enriched uranium (LEU), UO_2 prismatic block type fuel elements. Burnable poison rods are made of boron carbide (B_4C) [19], [21].

II.4.2 HTR-10

Figure II.8: The HTR-10 [18]

This 10 MW(th) pebble type reactor built at the Institute of Nuclear Energy and Technology (INET), in China achieved first criticality in 2000. The reactor core region consists of fuel and graphite spheres. The core is surrounded by a thick graphite reflector with holes for B_4C absorber balls. An equilibrium reactor core contains about 27 000 TRISO coated fuel particles with low enrichment UO_2 kernels. The average helium inlet and outlet temperatures are 250˚C and 700˚C respectively [19].

II.4.3 GT-MHR

The modular helium reactor is a technology opted for by the U.S culminating from almost 50 years of development of HTGR concept. This reactor type is developed by General Atomics. In this concept a high efficiency Brayton cycle gas turbine (GT) is coupled to a gas cooled modular helium reactor (MHR). The reactor employs TRISO coated fuel particles contained in a hexagonal prismatic fuel element. The design core inlet and outlet temperatures are 491˚C and 850 ˚C respectively with a net plant efficiency of 48% [19], [24].

II.4.4 PBMR

This prototype, a 165 MW(e) reactor will be built for ESKOM at Koeberg, South Africa. The graphite moderated, helium cooled reactor will employ the German type ceramic TRISO-coated spherical fuel "pebbles". This reactor will operate on a closed loop, direct Brayton cycle. A detailed description of this reactor is presented in Chapter I.

II.5 HTR FUEL IRRADIATION

This section gives an overview of the main fuel irradiation facilities and material irradiation testing reactors that played a major role in qualification of the HTR fuel (fuel compacts, spherical fuel pebbles and coated fuel particles). An overview of the fuel irradiation experiments performed and planned to take place at each of the facilities is also given. Irradiation experiments are conducted to assess the integrity of the fuel after it has been exposed to high temperatures, fast neutron flux and after reaching high burn-up levels. Results of these experiments can be used for licensing of the fuel manufacturing process, hence the fuel itself. From these experiments, data is obtained concerning particle failure fractions, fission product transport and fuel element integrity [25].

Different fuel types have been irradiated under U.S.A and German irradiation experiments. The main focus of the U.S.A fuel qualification was on the fuel compact fuel types: thorium/uranium carbide $(U/Th)C_2$, thorium oxide (ThO_2), and uranium carboxyl (UCO) and very little on uranium dioxide (UO_2) while the Germans qualified the thorium/uranium dioxide $(Th/U)O_2$ fuel with their main focus having been on the UO_2 fuel spherical fuel elements (pebbles) and coated fuel particles. [25].

The performance requirements of the fuel during this variety of irradiation experiments are to demonstrate [26], [27]:

- a fission product retention capability (with a fractional release of radioactivity below 10^{-4} during normal and accident conditions),
- high mechanical strength of the fuel element (through negligible release from fuel damaged due by the loading process and by interaction with control rods),
- high corrosion resistance from oxidizing agents (air, water, etc.) in the primary system (negligible compromise of retention of radioactivity and mechanical strength due to corrosion)
- sufficient dimensional stability and efficient heat transfer characteristics.

The AVR (pebble bed) and Dragon are the two experimental reactors that were used as test beds for a variety of HTR fuel and material irradiation experiments in Germany and the United Kingdom respectively. In the AVR, experiments were done to tests different fuel elements and demonstrate their safety, hence qualifying the fuel for high temperature operational conditions. The range of AVR experiments on spherical fuel elements include AVR 6 on LEU BISO/TRISO UO_2, AVR 14 and 18 on $(Th/U)O_2$ BISO, AVR 15 and 20 on $(Th/U)O_2$ TRISO, AVR 13 on UC_2 and ThO_2 TRISO, AVR 19 and 21 on LEU UO_2 TRISO. The experimental conditions for these experiments are very lengthy but can be accessed in [27]-[30]. In the DRAGON reactor, spherical fuel elements were irradiated in experiment DR-K5 with the LEU UO_2 BISO/TRISO. In the SILOE reactor, loose coated particles (LEU TRISO UO_2 fuel) and fuel compacts were also irradiated.

II.5.1 The High Flux Reactor (HFR)

The HFR at Petten in the Netherlands is a tank-in-pool type, multipurpose research reactor and has been used extensively for testing of high temperature gas-cooled reactor fuels and materials. It has been the workhorse for the irradiation of spherical fuel elements for the German HTR project for the period 1970-1995. The reactor is water cooled and moderated. It is operated at a power of 45 MW(th). The core lattice is a 9x9 array of 33 fuel assemblies, 6 control elements, 17 experimental positions and 23 beryllium reflector elements. For fuel irradiations, a wide span of high neutron flux in core positions to low and variable flux in the pool side facility is available. The fast neutron flux has of $4.5 \times 10^{18} n/m^2.s$ and thermal neutron flux of $2.4 \times 10^{18} n/ m^2.s$ are achieved [26].

Table II.1: Summary of the German LEU-TRISO Spherical Fuel Element Tests in the HFR [27]-[30].

Experiment	Fuel type and number of fuel elements	Irradiation time (efpd)[a]	Burn-up (%FIMA[b])	Fluence (E>0.1MeV) ($x10^{21}$ cm^{-2})	Temperature at centerline (°C)
HFR-K3	LEU UO_2-4	359	7.5-10.6	4.0-5.9	920-1220
HFR-K4	LEU UO_2-2	667	13	10	1250
HFR-K5	LEU UO_2-4	565	6.7-9.1	4.0-5.9	903-921
HFR-K6	LEU UO_2-4	634	8.34-10.88	3.2-4.8	1090-1140

[a] Effective full power days

[b] Fissions per Initial Metal Atoms

Irradiation of HTR fuel in the form of loose CFP and fuel compacts irradiation took place in the HFR of Petten under experiment HFR-P3 for HEU uranium carbide (UC) and thorium dioxide fuel, (ThO_2) and HFR-P4 for LEU uranium dioxide (UO_2) TRISO [27]-[30].

Table II.2: Summary of the Recent German LEU-TRISO Spherical Fuel Element Tests [32].

Parameters	HFR-EU1 bis (GLE-4 pebbles)	HFR-EU1 (GLE-4 pebbles)	HFR-EU1 (INET pebbles)
Number of pebbles	5	3	2
Particles/pebble	9560	9560	8500
Burn up (%FIMA)	16	≤20	≤17
Surface temperature (°C)	1000-1050 at BOL raised to maintain central temperature constant at 1250	950	950
Fluence (cm^{-2}) E>0.1 MeV	~5 x 10^{21}	<6 x 10^{21}	5.3 x 10^{21}
Fission power (W)	<3400 W/pebble <340 mW/particle	<2300 W/pebble <241 mW/particle	<1750 W/pebble <206 mW/particle

To date, the HFR reactor in the Netherlands is still serving as a workhorse for HTR fuel irradiations. HTR fuel was irradiated at the HFR of Petten in two experiments, HFR-EU1 and HFR-EU1bis, with the objective of exploring the potential for high performance and high burn-up of the existing pebble fuels for use in the pebble bed Very High Temperature Reactors (VHTR). In the HFR-EU1 experiment, three German-made HTR pebble fuel types and two Chinese pebble fuel types fabricated at the Institute for

Nuclear Energy Technology (INET) were irradiated. In the HFR-EU 1bis experiment, five German-made pebble fuel types and six mini samples containing 10 particles each were irradiated [31], [32]. *Table II.2* gives a summary of the main experimental requirements for both HFR-EU1 and HFR-EU1 bis.

II.5.2 The FRJ2 Reactor

FRJ-2 at Julich, is a DIDO class reactor, moderated and cooled by heavy water. The core is graphite reflected. The reactor started operating in 1962 at 10 MW(th), with a first power increase to 15 MW(th) in 1967 and to 23 MW(th) in 1972, accompanied by an upgrade and modifications. About 30 vertical tubes were available as facilities for fuel and structural material irradiations and facilities for isotope production and activation analysis. The reactor operated at thermal neutron flux of 2.9 x 10^{14} n/cm^{2}s and fast neutron flux of 2.2 x 10^{14}n/cm^{2}s [33]. This reactor facility was shut down in 2006.

The following loose CFP and fuel compact irradiation experiments were performed at this reactor: FRJ2-P27 and P-28 on LEU UO2 TRISO, FRJ2 P-22 and 25 on HEU (Th/U)O_2 BISO, FRJ P23 and 25 on HEU (Th/U)O_2 TRISO and FRJ2 P-25 on HEU UC/ThO_2 TRISO. A summary of the spherical fuel element irradiation is given in *Table II.3*.

Table II.3: Summary of the German LEU-TRISO spherical fuel element tests in the FRJ2 reactor [25], [30].

Experiment	Fuel type	Irradiation time (efpd)	Burn up (%FIMA)	Fluence (E>0.1MeV) (x10^{21} cm^{-2})	Peak temperature (°C)
FRJ2-K13/1	LEU UO_2	396	7.5	0.2	1125
FRJ2-K13/2			8.0		1150
FRJ2-K13/3			7.9		1150
FRJ2-K13/4			7.6		1120
FRJ2-K15/1		533	13.2		970
FRJ2-K15/2			14.6		1150
FRJ2-K15/3			13.9	0.1	990

II.5.3 The IVV-2M Reactor

The IVV-2M reactor is a pool type, 15 MW(th) research reactor commissioned in 1966. The reactor was built at the Institute of Nuclear Materials of Russia. It is light water cooled and moderated and beryllium reflected. The fuel assemblies consist of five tubular, three-layered hexagonal fuel

elements. The reactor thermal neutron flux is 5 x 10^{14} n/cm^2.s and the fast neutron flux is 2 x 10^{14} n/cm^2.s for E>0.1 MeV [34]. Fuel irradiations were planned in this reactor for the PBMR fuel.

Table II.4: Experimental conditions for the HTR fuel irradiation in IVV-2M reactor.

Experiment	Fuel type	Irradiation time (efpd)[a]	Burn up (MWd/tU)	Fluence (E>0.1MeV) (x10^{21} cm^{-2})	Temperature centerline (°C)
SFE 5	LEU UO_2	359	97 300	1.10	1000±50
SFE 7		625	107 000	1.31	
SFE 8		565	101 900	1.30	
SFE 12[c]		634	95 000	1.06	

[c] The temperature of fuel element was increased to 1200°C for 200 hours and 1250°C for 200 hours when burn-up levels of 38 700 and 57 300 MWd/tU were reached respectively.

Irradiation of the coated fuel particles and spherical fuel spheres was undertaken between 1982 and 1989 at the IVV-2M in the "KASHTAN", "RBT" and "VOSTOK" instruments to span a variety of irradiation conditions (temperature, burn-up and fluence) [35]. The IVV-2M reactor was also used in qualification testing of the Chinese INET fuel for use in the HTR-10 reactor. An irradiation testing experiment were conducted starting July 2000 ending February 2003 at the IVV-2M reactor with the objective of studying the irradiation performance of the INET fuel, following the operating conditions and design specifications of this reactor. The test consists of four spherical fuel elements each contained in an independent capsule with the fifth capsule containing loose coated fuel particles. The irradiation conditions [35]-[37] are given in *Table II.4*.

II.5.4 The BR2 Reactor

The BR2 material testing reactor in Mol, Belgium has been operated by SCK.CEN since 1963. The reactor core is contained inside an aluminum pressure vessel, located in a pool of demineralised water. The core is beryllium moderated and cooled by pressurized (12 bars) light water. The reactor is fuelled with high enriched (93%), plate-type uranium-aluminum alloy fuel. The fuel is clad with aluminum. Each fuel element contains 400g of ^{235}U and consists of six plates. A total of 79 channels are available for loading driver fuel, control rods and/or experimental devices. The reactor's nominal power ranges from 50-70 MW(th) depending on the core configuration used and the experimental requirements. The fast neutron flux reach a maximum of 3.5 x 10^{14} n/cm^2.s for E>1MeV and 7 x 10^{14} n/cm^2.s for E>0.1MeV. The thermal neutron flux is in the order of 10^{15} n/cm^2.s [38].

Three experiments were done in the BR2 reactor on HTR loose CFP and compacts: BR2-P25 on HEU (Th/U)O_2 TRISO fuel, BR2-P23 on HEU UC and ThO_2 TRISO fuel and BR2-P24 on HEU (Th/U)O_2 BISO fuel [27]-[30].

II.5.5 The R2 Reactor

The R2 reactor at Studsvik in Sweden is a 50 MW(th) tank type reactor. The reactor reached its first criticality in 1960. The core is light water cooled and moderated. The choice of reflectors for the core includes beryllium, heavy water and light water. The core contains six cadmium control rods with a fuel follower. The maximum steady state thermal and fast neutron flux in the core are both roughly 2.4 x 10^{14} n/cm^2.s [39]. The results of the spherical fuel elements irradiation experiments in the R2 reactor are given in *Table II.5*.

Table II.5: Summary of the German LEU-TRISO spherical fuel element tests in the R2 reactor [25].

Test	Fuel type	Irradiation time (efpd)	Burn-up (%FIMA)	Fluence (E>0.1MeV) (x10^{21} cm^{-2})	Temperature centerline (°C)
R2-K12/1	(Th,U)O_2	308	11.1	5.6	1100
R2-K12/2			12.4	6.9	1280
R2-K13/1		517	10.2	8.5	1170
R2-K13/2			9.8	6.8	980

II.5.6 The High Flux Isotope Reactor (HFIR)

The HFIR at the Oak Ridge National Laboratory (ORNL) is a light-water cooled, beryllium reflected reactor that employs high enriched uranium-aluminum (HEU U-Al) fuel to produce high neutron fluxes for material testing and isotope production. The reactor reached its first criticality in 1966. It has been used in the U.S. gas reactor programs to irradiate coated fuel particles. The reactor was used for fuel compact irradiation in the HRB-21 (which contained U.S.A fuel) and HRB-22 (which contained the Japanese fuel). These experiments were the last in the U.S. commercial program in the early 1990s [40], [41] and the irradiation conditions thereof are described below. The rest of the other irradiation experiments (HRB 4-6, HRB14-15 *etc.*) in this reactor will not be presented since the experiments focus on fuel compact irradiations rather than the pebble irradiation, which is the focus of this study.

In the HRB-21 fuel irradiation experiment three fuel compacts were irradiated for 105 days, the fast fluence spanned a range from 1.5 x 10^{21} cm^{-2} to 3.5 x 10^{21} cm^{-2}, the average irradiation temperatures ranged from 800°C to 1000°C while the burn-up levels reached a maximum of 22.5 %FIMA. The HRB-

22 experiment also involved irradiation of three fuel compacts with irradiation temperatures in the range of 1150°C to 1350°C, the fast fluence of 2.5 x 10^{21} cm^{-2} to 4.1 x 10^{21} cm^{-2} and burn-up of 7.0 to 9.5 %FIMA.

II.5.7 The OSIRIS Reactor

The OSIRIS in Saclay, France, is a 70 MW(th) reactor moderated by light water. The reflectors are a combination of light water and beryllium. It is an experimental pool type reactor fuelled with LEU (19.75%) U_3Si_2-Al plates. The core consists of 38 fuel elements and 6 hafnium control rods. The reactor thermal neutron flux is 5 x 10^{14} $n/cm^2.s$ and 4.5 x 10^{14} $n/cm^2.s$ for the fast neutron flux (E>0.1 MeV). A variety of irradiation positions allows for irradiation of HTR fuel compacts and free particles [42], [43].

HTR fuel compacts irradiation experiments were planned in this reactor. These irradiation experiments also fall out of the scope of this study and will only be presented briefly. The objectives of these tests are to verify the quality of the fuel integrity and fission product retention capability and to verify the ability of the reference fuel to withstand the VHTR conditions. The SIROCCO 1 experiment was scheduled for June to December 2006, for irradiation of fuel compacts for about 150 days to reach a fuel surface temperature of 1250°C and fast fluence greater than 2 x 10^{21} cm^{-2}. In the SIROCCO 2 experiment, planned for June 2007 to December 2008, the fuel compacts are to be irradiated for up to about 450 days, to reach a burn-up of approximately 15 %FIMA with target fuel surface temperatures of about 1000°C to 1200°C.

II.5.8 Advanced Test Reactor (ATR)

The ATR at the Idaho National Engineering and Environmental Laboratory (INEEL) in the U.S.A, is a light-water cooled, beryllium reflected reactor that uses the HEU U-Al in a four-leaf clover configuration to produce high neutron fluxes for material testing and isotope production. This configuration boosts nine very high flux positions, termed flux traps. Other holes of varying sizes are available for testing and for irradiation of coated particles. The core consists of 40 U/Al fuel assemblies. The reactor thermal fluxes are in the range of 2 x 10^{13}-1 x 10^{15} $n/cm^2.s$ while the fast flux (E>1 MeV) is the range of 3 x 10^{12}-5 x 10^{14} $n/cm^2.s$ [44].

In the U.S.A, irradiation testing of the UCO fuel to be used in the Advanced Gas Reactor (AGR) has started. Irradiation of the variant fuel compacts is underway at the ATR. The test objectives are: to produce data on fuel performance under irradiation, support development and validation of fission transport fuel performance models and codes and provide irradiated fuel for post irradiation examination (PIE) and accident testing. The experiment consists of eight irradiation capsules [44] and is also out of the scope of this study.

II.5.9 The SAFARI-1 Reactor

The SAFARI-1 reactor at Necsa, Pelindaba in South Africa, was commissioned in 1965 and is a material testing reactor (MTR). It is a 20 MW(th) tank-in-pool type reactor of the Oak Ridge design. The SAFARI-1 reactor is has an 8 x 9 core lattice. The grid has nine columns (1-9) and eight rows (A-H) as shown in Figure II.*9*.

The core lattice houses 26 MTR type fuel elements each containing, 19 U/Al alloy fuel plates, five control rods, one regulating rod, in-core irradiation facilities, and a number of aluminum and beryllium reflector. The reactor employs light water as a moderator and coolant. A conversion study for the core, from HEU (90%) U-Al alloy fuel to LEU (19.75%) silicide U_3Si_2 fuel has been done and is now in the implementation stage [45]. This reactor boasts a variety of irradiation in-core and ex-core, some of which can be accessed during reactor operation and some only at shutdown.

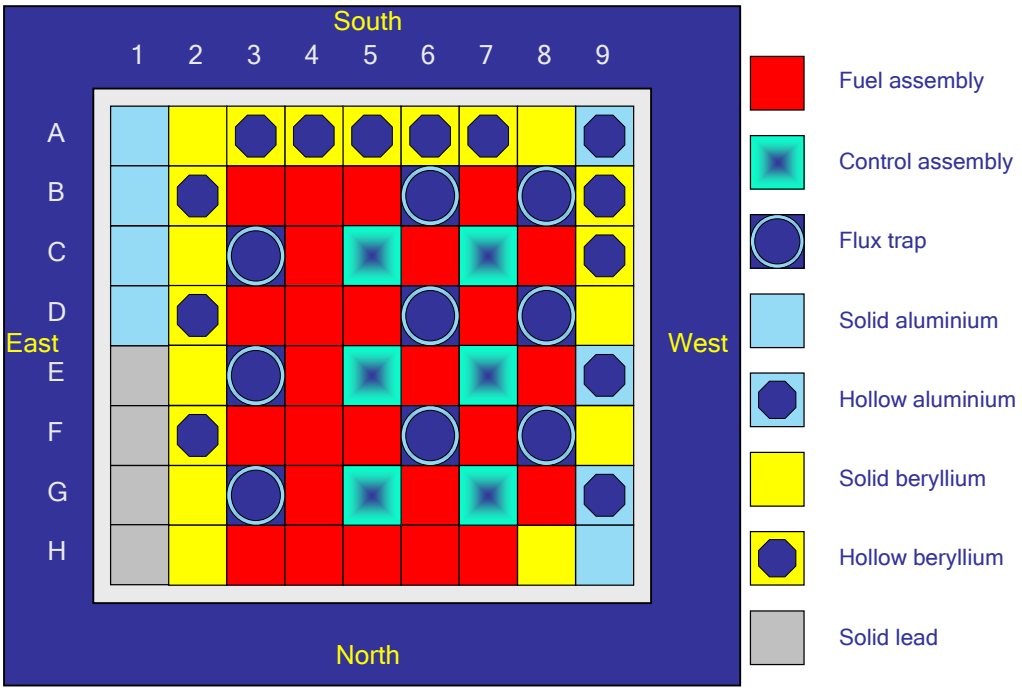

Figure II.9: SAFARI-1 Core Layout

II.5.9.1 The PBMR Fuel Irradiation Program

Plans are underway to have the Necsa fabricated PBMR fuel (loose CFP's and spherical pebble fuel) irradiated at the SAFARI-1 reactor in Pelindaba. The desired irradiation parameters for the PBMR fuel [32] are:

- A target burn-up of ~10% FIssion per Initial Metal Atom (FIMA)
- A target neutron fluence of 2.4 x 10^{21} cm^{-2} (E>0.1 MeV),
- A maximum fuel surface temperature of 1000C
- A maximum fuel centerline temperature of 1100C,
- Maximum fission power per pebble of 3.4 kW and 4.5 kW for equilibrium and first core respectively,
- Maximum fission power per particle of 250 mW and 300 mW for equilibrium and first core respectively,
- Irradiation time of 900 efpd

CHAPTER III : CALCULATIONAL TOOLS

III.1 INTRODUCTION

The design and analysis of a nuclear reactor and the optimization of the in-core fuel cycle require the availability of suitable neutronic codes. The PBMR introduces several challenges for core neutronic methods. The TRISO coated fuel is highly heterogeneous with a random distribution within the fuel pebbles. The complete solution of the core physics problem must simultaneously account for: movement of the fuel (refueling/shuffling), composition of the fuel as it is burned, flux distribution in the core and spatial variation of composition.

In this chapter, the neutron transport equation is briefly presented in section III.2. The rest of the chapter describes the theory and limitations of the three codes that are used in this work. The order will be from OSCAR-3, MCNP5 to OSMINT in subsections III.3, III.4 and III.5 respectively.

III.2 THE NEUTRON TRANSPORT EQUATION

In general, the behaviour of a neutron is described by the neutron density $n(\underline{r},E,\underline{v},t)$, which is a function of a spatial position r, energy E, the velocity v and time t where often the angular density $n(\underline{r},E,\underline{\Omega},t)$ is used instead of the velocity. The time dependent neutron transport equation is presented below only accounting for the formation of prompt neutrons due to fission [47], [48]:

$$\frac{1}{\upsilon}\frac{\partial}{\partial t}\psi\left(\underline{r},E,\underline{\Omega},t\right)+\Sigma_t\left(\underline{r},E\right)\psi\left(\underline{r},E,\underline{\Omega},t\right)+\Omega\bullet\nabla\psi\left(\underline{r},E,\underline{\Omega},t\right)$$
$$=\int_0^\infty dE'\int_{4\pi}d\Omega'\Sigma_s\left(\underline{r},E'\to E,\underline{\Omega}'\to\underline{\Omega}\right)\psi\left(\underline{r},E,\underline{\Omega},t\right)$$
$$+\frac{\chi_{\mathrm{p}}E}{4\pi}\int_0^\infty dE'\int_{4\pi}d\underline{\Omega}'\upsilon(E')\Sigma_f\left(\underline{r},E'\right)\psi\left(\underline{r},E',\underline{\Omega}',t\right)$$
$$+\mathrm{Q}_{\mathrm{ext}}\left(\underline{r},E,\underline{\Omega},t\right)$$

III-1

The first term on the left hand side represents the time rate of change of the neutron population in a volume V, the second term is the rate of loss of neutrons in V due to collisions and neutrons leaving the system by absorption or scattering out. The third term represents the net leakage rate of neutron through a surface S. On the right hand side, the first term represents rate of neutron entering the volume V due to in-scattering from different energies and directions, the second term is the rate at which prompt fissions are born in the volume while the third term is the rate of neutrons born from external sources in a volume V. In the equation $\psi\left(\underline{r},E,\underline{\Omega},t\right)$ is the angular neutron flux which is equal to $\upsilon(E)n\left(\underline{r},E,\underline{\Omega},t\right)$ where

$n(\underline{r}, E, \underline{\Omega}, t)$ is the energy dependent neutron angular density, Σ_t, Σ_s and Σ_f are the total, scattering and fission macroscopic cross sections respectively, χ_p is the energy distribution spectrum of the prompt fission neutrons and $\upsilon(E)$ is the total number of neutrons produced per fission event.

The methods of solving the neutron transport equation can be divided into two classes: the deterministic and Monte Carlo (MC) methods. The deterministic methods, solves the BTE for the average particle behaviour by calculating the neutron fluxes and providing information on every single cell in the geometry. On, the contrary, the MC methods does not solve the BTE explicitly instead it simulates the particle behaviour through a random walk process and records some aspects of its behaviour (tallies). The MC methods only give information on what the user has requested as tallies [47], [48].

The class of deterministic methods includes the finite difference, finite element, the P_N method and discrete ordinate (S_N) methods. The P_N multi-group method solves the BTE by expanding the angular dependence of the neutron flux in spherical harmonics using a series of Legendre polynomials. This series is truncated or made to be finite to allow for efficient and realistic solutions. The spatial dependence of the neutron flux is handles through discretization of phase space into points, while the energy domain is also discretized into a finite number of energy intervals, where each energy interval is called a group. The difference between the two multi-group approximations, P_N and S_N is that in the latter, the BTE is solved in a solved in a discrete set of directions only – no spherical harmonics employed. In the S_N approximation, all the independent variables in the steady state BTE, namely space, energy and angle are treated as discrete. A discrete energy variable is introduced using the multigroup approximation and discrete space mesh is used for all spatial coordinates [47], [48].

Two categories are realized for the discretization of the spatial domain: the fine mesh and coarse mesh methods. In the fine mesh methods or finite difference methods, spatial domain is divided into very small spatial meshes, about one mean free path in each dimension. The coarse mesh methods or nodal methods are based on the high-order or analytical expansion solution in the spatial variable and are applied to meshes far larger than the mean free path. These methods are restricted for application to spatial meshes which contain homogeneous material (i.e. requires homogenization of the spatial domain). On the contrary, Monte Carlo methods do not suffer any restriction as far homogenization is concerned; this method can in fact handle very complicated heterogeneous systems [47], [48].

The steady-state Boltzmann transport equation is solved to obtain steady-state directional neutron flux. In this work, only the steady state, time-independent calculations are sought.

III.3 DESCRIPTION OF THE CODE SYSTEMS

III.3.1 OSCAR-3

OSCAR is an acronym for an "Overall System for the CAlculation of Reactors". The code system has been developed at Necsa over many years. The OSCAR-3 code package, based on three dimensional nodal diffusion methods, is used to perform core follow calculations in few groups making use of the homogenized assembly cross sections. In OSCAR-3, a deterministic approach is followed for solving the neutron transport equation. This simplifies the problem since time is divided into discrete time points, energy is split into a finite number of energy groups, space is divided into a number of volumes (nodes) and the angle is divided into a finite number of directions or integrated. OSCAR-3 consists of four sub systems: MAESTRO, CROGEN, CROLIN and CORANA [12], [49] as shown in below *Figure III.1* below. A brief description of each of these subsystems will be given.

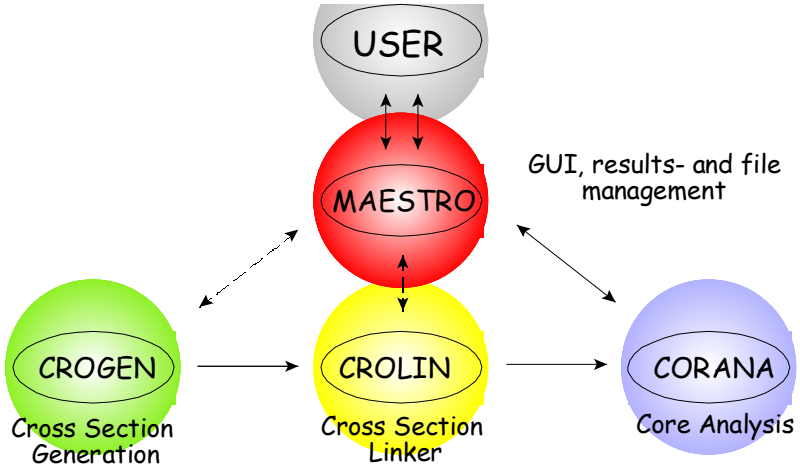

Figure III.1: OSCAR-3 subsystems

III.3.1.1 MAESTRO

MAESTRO is a graphical user interface for the OSCAR-3 system. Although currently linked to CORANA, it is meant to control all the sub systems. It consists of the following programs: config editor, exposure editor, shuffle, mcgrac, results viewer and report generator [12], [49].

III.3.1.2 CROGEN

CROGEN is the cross section generation system of OSCAR-3. It contains the following codes: HEADE, STYX, DUCO and EQUIVA for creating few group cross sections data. HEADE is a code in OSCAR-3 based on low order current interface formalism. It is used to create homogenized cross sections for fuel assemblies, reflectors and other simpler geometries (e.g. plate type or cylindrical fuel elements). Some geometries are very difficult to be modeled with HEADE, and then STYX comes into play. STYX is used

to create homogenized cross sections for complex geometries like complex irradiation rigs. DUCO creates cross sections for control rods consisting of both an absorber portion and a fuel portion (i.e. control rods with fuel follower). And lastly, EQUIVA is used to create cross sections for the reflectors, the regions in which the diffusion theory is invalid [12], [49].

III.3.1.3 CROLIN

CROLIN is the cross section linker. It reads output from CROGEN calculations and converts it into a file format that can be used for core calculations. The following codes are included in the CROLIN subsystem: POLX, LINX and RECONS. POLX converts the exposure and state-dependent few group nodal data (burn up chains, cross sections, isotopic data etc.) into a quadratic polynomial representation. LINX combines assembly or reflector POLX files into a run time file to be used by MGRAC and/or SHUFFLE in core analysis. RECONS process polynomial data on a LINX file to perform depletion calculations and produce few-group nodal parameters at specified exposures and physical states [12], [49].

III.3.1.4 CORANA

CORANA is a core analysis module of OSCAR-3. It consists of MGRAC, a multi group analytic nodal diffusion code. SHUFFLE is also a sub code in CORANA, which allows for the loading and unloading of the reactor for cycle analysis [12], [49].

III.3.2 Monte Carlo Code Systems (MCNP5) [13]

The Monte Carlo methods emerged from work done at Los Alamos during World War II. It is a non-analytical, powerful, versatile and highly accurate method. The MC methods do not solve an explicit equation but rather obtains answers by simulating the interactions between the particles in some defined geometry. Monte Carlo methods are very useful in solving complex problems that cannot be solved with the deterministic codes.

Monte Carlo methods use random numbers to determine the outcome of the life of a particle. In this method, a particle is tracked from its birth to its death through a series of interactions, using random numbers generated to sample the particle mean free path, and the type of interaction (scattering, fission, capture, leakage *etc*.) it will undergo, *etc*. Each interaction of the particle is recorded and weighted accordingly, to form so called particle histories. As more such histories are followed, the neutron and photon distribution is known better and the accuracy of the sampling becomes better. The desired results are tallied together with their statistical error estimates.

MCNP is shorthand for Monte Carlo N-Particle code. The code is developed and owned by the Los Alamos National Laboratory (LANL). MCNP is a general-purpose Monte Carlo radiation and protection code used for calculating the time-dependent continuous energy transport of neutron, photon, electron and coupled neutron/ photon/ electron problems. Both the fixed source and criticality problems can be solved. This code is capable of modeling and transporting particles in complicated geometries, with no necessity to approximate geometries. A geometry plotting capability allows for errors in the geometry set-up of the input file to be checked.

The problem with deterministic codes is that intricate three dimensional (3-D) geometries cannot be modeled accurately. The present generation of deterministic 3-D radiation and protection codes also generated intermediate results in "scratch files" that easily grow to 1000 Giga Byte (GB) in size. Monte Carlo codes do not suffer from such limitations.

III.3.2.1 MCNP5 Concepts and Features

The general structure of the MCNP input, namely cell, surface and data cards as well the tallies are described below. An MCNP input file for the pebble and the rig model is included in the Appendix and the discussion below is made with reference to some lines extracted from this file.

A. GEOMETRY MODELING

i. The Surface Cards

The surface card describes the problem geometry in terms of:

- planes: cutting any of the axis (px, py and pz), parallel to any of the axis (p/x, p/y and p/z),
- spheres: centered at the origin (so) or on any of the axis (sx, sy and sz),
- cylinders centered on any of the axis (cx, cy and cz), parallel to any of the axis (c/x, c/y and c/z)
- and macro bodies (box, rectangular parallelepiped (rpp) and right circular cylinders (rcc), etc.

These surfaces are used to construct the problem cells. In the example below, a sphere centered at the origin, with a radius of 2.5 cm and another sphere also centered at the origin with a radius of 3 cm are defined.

```
c pebble surfaces
770   so    2.5                    $ fuel region
771   so    3.0                    $ non-fuel graphite region
```

Any text to the left of "c" in MCNP is seen by the code as a comment. In the second and the third line, the first entry is the surface number, the second entry is a surface type, in this case a sphere centered at the origin with the dollar ($) sign also representing a comment in MCNP.

ii. The cell cards

The cells are defined in the cell card by a logical combination (using intersections – represented by a blank space, and unions – represented by a semicolon) of the surfaces provided in the surface card. This card specifies the material that fills a particular cell, as well as its density. An example thereof is given below:

```
c coated particle lattice cells
861   0  -761 764  -760 763  -765 762 -767 766   lat=2   fill=50  &
                                                  u=52  imp:n=1  $ infinite
c pebble cells
870   0                      -770      fill=52    u=54   imp:n=1  $ fuel region
871   505   8.72390e-02    770 -771            u=54   imp:n=1  $ non-fuel region, graphite
872   505   8.72390e-02    771              u=54    imp:n=1  $ graphite insert for a pebble
```

The first entry in a cell card is the cell number. The second entry is the material number which is provided in the material card described in the data cards section of the input file. The third entry is the atom density (atom/barn-cm) if the entry is positive and otherwise gram density (g/cm^3) if the entry is negative. The fourth entry defines the cell boundaries using the surfaces entered in the surface card, where the negative sign in front of the surface number represents the surface sense. In case of general surfaces a negative sign indicate anything to the left or below the surface while a positive sign represents anything to the right or above the surface. In case of macro bodies a negative sign indicated the inside of the surface while a positive sign represents the outside of the surface.

Complicated geometries are modeled using repeated structure options together universe and fill cards. In the definition of cell 870 above, for example, filled with universe 52 (u=52) where this universe describes an infinite triangular lattice (lat=2). The other lattice type option is lat=1, which represents a square lattice. The surfaces that bound this lattice are created as prescribed in [50]. In MCNP, when the cell number (as in cell 870 above) is followed by a zero then it means that it is going to be filled with some universe defined in some prior cells or it is a void cell if its importance is zero.

iii. The Importance Cards

In the description of the cell card above (with reference to the second line), the seventh entry is the importance card, which tells the code in which cell(s) to terminate the particle history. The cell importance is also used for variance reduction techniques such as splitting and Russian roulette to help particles move to cells of higher importance. It indicates the importance of a cell to neutrons, or to photons (if imp: p) or electrons (if imp: e). If a particle enters a cell of zero importance (imp: n =0), then MCNP does not follow or track it anymore. Otherwise the importance card can be omitted in the cell card input line and put in the data card section as imp:n 1 1 1 1 1 0, meaning that the first five cells have a

neutron importance of one and only the last cell a zero importance. It is, of course more "intuitive" to put importances in the specific cell cards.

B. Data Cards

i. Material Cards

The data cards contain many types of cards, such as for example: the material card, in the form of ZAID.nn. The ZAID part contains the atomic number Z of the isotope followed by its atomic mass M. The nn part contains a choice of cross section for evaluation, where nn specifies the library number, a final c = continuous cross section, a final d = discrete cross section and a final m = multigroup cross section library. Using UO_2 fuel as an example, a typical material card entry will be:

```
m500  92235.66c  2.37e-03   92238.66c  2.17e-02   8016.66c  4.82e-02    $ UO2 kernel
```

The first entry is the material number followed by the ZAID.nn entry. The third entry is the atom density (positive entry) in the unit of atoms per barn centimeters (atom/barn-cm) or gram density (negative entry) in the unit of g/cm^3. The S(α,β) treatment discussed in the cross section library section below is invoked by the identifiers on the MTn card, where n is the material number.

ii. Source Cards

The source is described as either SDEF or KSRC (used in criticality calculations). In a criticality calculation, the source card takes a form such as, for example:

```
KCODE  5000   1.0   25   325
KSRC   0  0  0
```

The first line tells that a total of 5000 particle histories will be followed with an initial guess of the multiplication factor =1, skipping 25 cycles to allow for source convergence and running a total of 325 cycles. Tally calculation only starts after the first 25 cycles are done. KSRC indicates a series points (x_1, y1, z1; x_2, y2, z2, etc) in which the fission source lies, and are picked at random with a recommendation that at least one point should be in the fissionable region of the geometry.

In a general source definition (SDEF), the user specifies the position (pos) of the neutron, photon or electron source (x, y, z) and the energy (erg). The radial distance (rad) from pos of the source is also specified for cylindrical and spherical sources. The distance from pos along axs (ext), normally the range (height) of the source in cylindrical sources and the axs-a reference are also specified.

```
SDEF   cel=10   pos= (0 0 0)
```

The energy spectrum can be specified by the SPn and SIn cards using built-in functions for source probability. When the energy is not specified, then the default 14 MeV neutron energy is used in MCNP.

iii. Physics Treatment Card

Incorporated in the MCNP code is different physics treatment capabilities for neutrons, photons and electrons. Use of these cards determines which particle interactions (Coherent and incoherent scattering, pair production and annihilation, photoelectric effect, bremstrahlung effects, etc) to be tracked and tallied. Source particles are transported in the geometry through an analog or implicit capture process as defined on the PHYS:n and CUT:n cards – n being the particle designator which can either be neutron (n), photon (p) or electron (e).

C. TALLIES

The **tally card**, describes the type of answers required by the user. This can be the surface current (F1), surface flux (F2), track length estimate of cell flux (F4), flux at a point detector or ring detector (F5), track length estimate of energy deposition (F6), track length estimate of fission energy deposition (F7) or pulse height tally (F8). Only the tallies that are applicable in this particular work will be explained in the subsection below. These include the F4, F6, F7 and F8 tallies.

i. F4 TALLY

The F4 tally represents the average particle flux in a cell and can be written as:

$$\overline{\phi_V} = \frac{1}{V}\int dE \int dV \int ds\, N\left(\bar{r}, E, t\right) \qquad \text{III-2}$$

Where $N(\bar{r}, E, t) = \int d\Omega\, n(\bar{r}, \bar{\Omega}, E, t)$ is the number density of the particles and $d\bar{s}$ is the differential track length noting that $d\bar{s} = \bar{v}dt$. The quantity $N(\bar{r}, \mathrm{E}, \mathrm{t})\,\mathrm{ds}$ may be taken as a track length density, thus the average flux can be estimated by summing track lengths. MCNP estimates the average particle flux by multiplying the particle weight W with the track length T_l in centimeters and dividing by the cell volume V in cm^3, that is $\frac{WT_{l_1}}{V}$.

The reaction rates in a cell are calculated by modifying the F4 tally with a FM card whereby the equation $\int \varphi(E)\,dE$ is changed into $\int R(E)\varphi(E)\,dE$, where $R(E)$ is a response function, which can be combination of the sum or product of the energy dependent quantities available in MCNP. The modified

F4 flux tally in MCNP is then $C\int \varphi(E)R(E)dE$, where the constant C is an arbitrary scalar quantity that can be used for normalization, it can for example be a number density and $\varphi(E)$ is the energy dependent flux from the F4 tally. The syntax for a tally multiplier card in MCNP is:

FMn (C m R)

Where n is the tally number for the cell in which the reaction rate is calculated, C is a constant, m is the material number entered in the material card and R is the reaction number. A list of the reaction numbers important and used in this work are listed below.

Table III.1: MCNP reaction numbers used with the FM tally modifier [13].

Reaction number	Reaction cross section description
Neutrons	
-4	Average heating number (MeV/collision)
-5	Gamma ray production cross section
-6	Total fission cross section
-8	Fission Q-value (MeV/fission)
Photons	
-5	Total cross section
-6	Photon heating number

ii. F6 TALLY

The F6 tally is the track length estimate of energy deposition in a cell in the unit of MeV/g. The tally can be used in a neutron only problem (MODE n), photon only problem (MODE p) and coupled neutron photon problem (MODE n p).The F6 tally represents a physical quantity:

$$H_t = \frac{\rho_a}{m}\int dE\int dt\int dV\int d\Omega\,\sigma_t(E)\,H(E)\,\psi(\bar{r},\bar{\Omega},\mathrm{E},\mathrm{t}) \qquad \text{III-3}$$

MCNP scores for the track length estimate of energy deposition in a cell by multiplying the particle weight W with the track length T_l in centimeters, the total cross section σ_t, the heating number $H(E)$ and the ratio of the atom density ρ_a in atoms/barn-cm to the cell mass m in grams in a relation given as:

$$W\,T_l\,\sigma_t(E)\,H(E)\frac{\rho_a}{m}.$$

iii. F7 TALLY

The F7 tally is the track length estimate of fission energy deposition in the unit of (MeV/g) in a cell that can be used in neutron only problems (MODE n).

$$H_f = \frac{\rho_a}{m} Q \int dE \int dt \int dV \int d\Omega \, \sigma_f(E) \, \psi(\bar{r}, \bar{\Omega}, \mathrm{E}, \mathrm{t}) \qquad \text{III-4}$$

MCNP scores for the F7 tally in a relation: $WT_l \sigma_f(E) Q \frac{\rho_a}{m}$ where the particle weight (W) is multiplied by the track length T_l in centimeters, the fission cross section σ_f and the fission heating Q-value Q in MeV and the ratio of atom density ρ_a in atoms/barn-cm to cell mass m in grams.

In MCNP5, the F6 tally is used as a track length estimator of energy deposition in a cell while the F7 tally is used as a track length estimate of the fission energy deposition in a cell. The F7 tally can only be used in a neutron-only mode (MODE N) MCNP run, because only neutrons cause fission in fissionable materials. This tally include gamma heating because photons are deposited locally. The F6 tally can be used in a neutron-only problem (MODE N), photon-only problem (MODE P) or coupled neutron/photon problem (MODE N P). In a MODE N problem, the F6 tally does not include gamma heating because photons are not transported. Therefore for fissionable materials F7: N>F6:N.

True heating can be obtained by summing up the F6 tally in MODE N and MODE P or else running a MODE N P calculation with F6: N, P tally as shown in the equation below:

$$\text{True heating} = \text{F6:N} + \text{F6:P} = \text{F6:N P} \qquad \text{III-5}$$

The F7:N tally gives the correct heating of fissionable materials if in the physical experiment no photons comes from somewhere else while the F6:N tally gives the correct heating of light materials only if in the physical experiment all the photons escape the system. The F4 tally representing the track length estimate of the cell flux can be modified using tally multipliers (FM card) in MCNP to be equivalent to the F6 and F7 tallies.

F4:N 10
FM4 ρ M 1 -4

F14: N 10
FM 14 ρ M -6 -8 III-6

F24: P
FM24 ρ M -5 -6

The above equation gives examples of using the tally modifier (FM card). In the equation ρ is the ratio of atom density (atoms/barn-cm) to mass density (g/cm^3) Using -1/ρ_g (ρ_g is the mass density) instead of this ratio also yields the same answer. M is the material number in cell 10. The rest of the entries are the reaction rate numbers and microscopic cross sections given in *Table III.1*.

D. TALLY NORMALIZATION

In MCNP5, tallies are normalized per source particle except in criticality calculations. The flux tally will then be in the units of $\frac{\text{neutrons}}{\text{cm}^2\text{source particle}}$, and this will give the correct spectral shape of the neutron scalar flux but not the correct magnitude in the units of $\frac{\text{neutrons}}{\text{cm}^2\text{s}}$. The normalized flux can be calculated using the average number of neutrons produced per fission (υ), the reactor operating power (P in MW), and the MCNP flux tally (φ) normalized per source neutron:

$$\varphi = \frac{\varphi_{MCNP}\upsilon P}{Q_{avg}}\left(\frac{10^6 W/MW}{1.6022\times10^{-13} J/MeV}\right) \qquad \text{III-7}$$

Typically for a uranium fuel reactor υ~2.43 and Q_{avg} ~200 MeV, then:

$$\varphi = \varphi_{MCNP}\times P\times 2.43\left(\frac{neutrons}{fission}\right)\left(\frac{1MeV}{1.6022\times10^{-13}J}\right)\times\left(\frac{fission}{200MeV}\right) \qquad \text{III-8}$$

The power (P) in equation III-9 is in the units of $\frac{Joules}{Seconds}$ to give the normalized flux in the correct unit of $\frac{\text{neutrons}}{\text{cm}^2\text{s}}$.

E. CROSS SECTION LIBRARIES

MCNP uses continuous energy nuclear and atomic data libraries with the primary sources being the Evaluated Nuclear Data File (ENDF), Evaluated Nuclear Data Library (ENDL), etc. These data libraries are created from evaluated cross section data files based on experimental results and theoretical models. Cross section libraries for neutron reactions are isotope-specific, meaning that each isotope has its own set of cross sections. For electron and photon reactions, the cross section data is atom-specific. Both the free and thermal $S(\alpha,\beta)$ treatments are used. The $S(\alpha,\beta)$ model accounts for the up and down scatter of neutrons when interacting with other particles at thermal energies. This model describes the moderating properties and the $S(\alpha,\beta)$ data for light water and graphite is used in this work.

F. ERROR ESTIMATION AND ACCURACY

An MCNP output file contains a tally result together with the estimated relative error. This relative error is defined as the standard deviation of the mean divided by the estimated mean. The accuracy of the calculations increases as the number of particles used in the simulation increases. Generally the error reduces as $1/\sqrt{N}$ (i.e. the root of the number of particles). An output file also contains a section which shows the ten statistical checks made for each tally to determine its convergence.

There are advanced techniques to reduce the statistical error and improve the efficiency of the calculation. Rapid convergence is enabled by using a variety of variance reduction techniques. The techniques are applied by ensuring that particle histories contributing to the results are sampled in favour of those that contribute less. Variance reduction techniques are very important in deep-penetration problems where radiation moves through very thick shields, or streams through long, narrow ducts. In the case of an in-core rig, variance reduction methods are not critically important, so that this study will not focus much on such techniques.

III.3.3 OSMINT [14]

Oscar-Mcnp INTerface (OSMINT) is a tool linking the core-follow and depletion code system OSCAR and the Monte Carlo code MCNP. It is a tool used to build the SAFARI-1 MCNP model via detection of the whole core configuration and isotopic inventory from OSCAR-3, thereby presenting a core that is accurate in both space and time. *Figure III.2* below is representative of a calculation scheme for OSMINT.

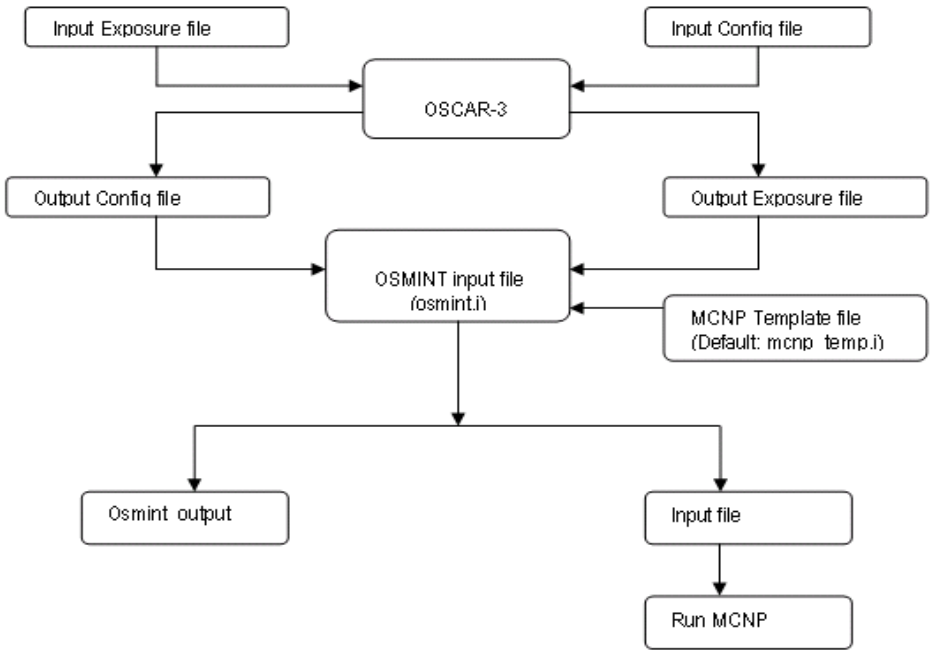

Figure III.2: Calculational path for OSMINT

In order to run OSMINT, the user needs the config file (a file from OSCAR-3 that contains information on the structural geometry of the core) and an exposure file (a file from OSCAR-3 that contains the material composition of the core in terms of number densities).

OSMINT has a capability to detect both the low enrichment uranium (LEU) and high enrichment uranium (HEU) fuel in the reactor core. It can also detect the control rod with a fuel follower and molybdenum in molybdenum rigs inserted in the core. A typical OSMINT input file is given in *Table III.2*.

Table III.2: Typical OSMINT Input data set

```
Option required:
3  represents Oscar-3(No coupling, Approximate Molly)
35 only to study Oscar-3 coupling approximation (Bank pos. at middle of coupling)
4  represents OSCAR-3 (Coupling; Bank pos at Cd tip, Exact molly model)
5  represents Exact Safari-1 physical core
                                        : 5
-----------------------------------------------------------
Exposure file name                      : Mo99.C0704-1.X0
Config file name                        : COREm.FIG
Cross-section directory file name       : xsdir
MCNP input file name                    : 0704.i
--
For non-active fuel zone--
Number of nodes at the top              : 2
Number of nodes at the bottom           : 2
-----------------------------------------------------------
Molly Control -
Insert the active fuel Al
combination for each Molly
Number of Molly devices                 : 6
                B8                      : 1  1  1  1  1  1  1
                C3                      : 1  1  1  1  1  1  1
                D8                      : 1  1  1  1  1  1  1
                E3                      : 1  1  1  1  1  1  1
                F8                      : 1  1  1  1  1  1  1
                G3                      : 1  1  1  1  1  1  1
-----------------------------------------------------------
For the number of control banks         : 2
Withdrawal distance (notches)           : 3396 3396
```

The input file is divided into five sections. The first section describes the four options and their particular use. For this study, option 5 is selected as it gives the exact SAFARI-1 core model. The exposure and config files are obtained from the output of OSCAR-3 and their names entered in the second section of the input file. The two files should also be located in the same directory subroutine from where OSMINT is run. The names of the cross section directory file should also be provided together with the desired name for the MCNP file name. This file is generated upon executing OSMINT and should be executable in MCNP without any modifications to ensure that OSMINT was run properly.

In OSCAR-3, the fuel plate is divided into 17 axial nodes, two inactive (not containing fuel) at the top and bottom of the plate. This is presented in section three of this input file. Section four gives information on the molybdenum devices in the core and only when OSMINT runs, will it detect if there is any molybdenum in those positions, and its mass in grams. The last section gives information on the control rod positions and can be user-modified.

OSMINT performs the following verifications:

- Isotopic transfer from OSCAR-3 to MCNP in terms of material identification (for example an exposure file identification for an isotope will be 92235U235, the HEADE identification will be U235 while the MCNP identification will be 92235.
- Volumes, masses (that is nuclide masses per node per plate per physical channel together with the thereof) and the gram densities calculated with OSMINT and MCNP.

After executing OSMINT, the user needs to execute all the outputs without any modification with regard to the cells, surfaces and material cards.

CHAPTER IV : MODELING AND SIMULATION

IV.1 INTRODUCTION

This chapter focuses on the geometry modeling of the PBMR coated fuel particle (CFP), the pebble fuel with thousands of CFPs embedded in it, the preliminary fuel irradiation rig and the SAFARI-1 reactor core. The accurate modeling of these geometries is a task that requires very detailed engineering drawings together with the material composition of each region. MCNP5 is used in this study for the purpose of modeling. The capability of MCNP5 to model complicated geometries using lattice and universe features became very useful in this section.

IV.2 MODELLING

IV.2.1 Model of a Pebble

The modeling of the pebble fuel poses a challenge due to the double heterogeneity of the fuel and the random distribution of CFPs in the fuel region of the pebble. The CFPs and the pebble are modeled using the dimensions and material specifications in *Table I.1* in Chapter I. In the CFP model, all the TRISO coating layers including the fuel kernel and the buffer layer are modeled explicitly as shown in *Figure IV.1*.

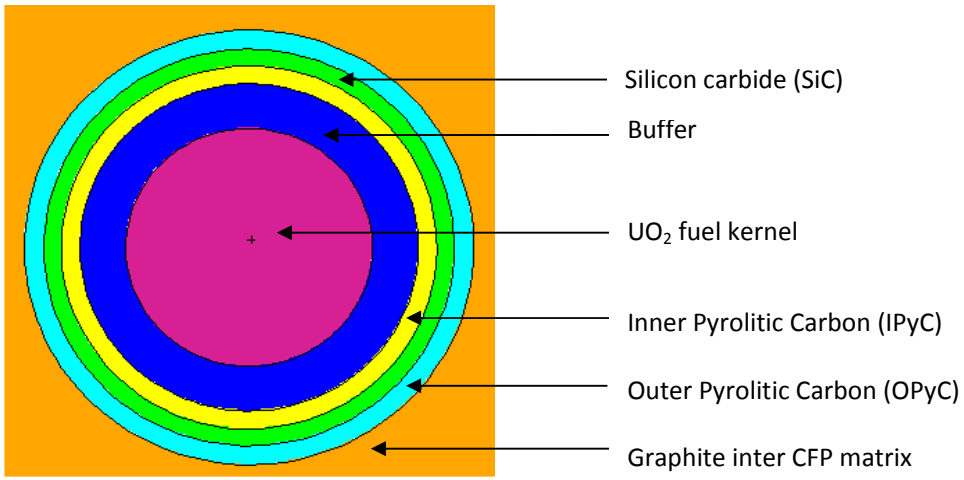

Figure IV.1: MCNP5 model of the CFP.

The random distribution of the CFPs in the fuel region is approximated using the lattice handling capability in MCNP5 [50]. A three dimensional (3D) hexahedral (triangular) lattice is chosen for this study, modeled in MCNP5 and presented in *Figure IV.2* below.

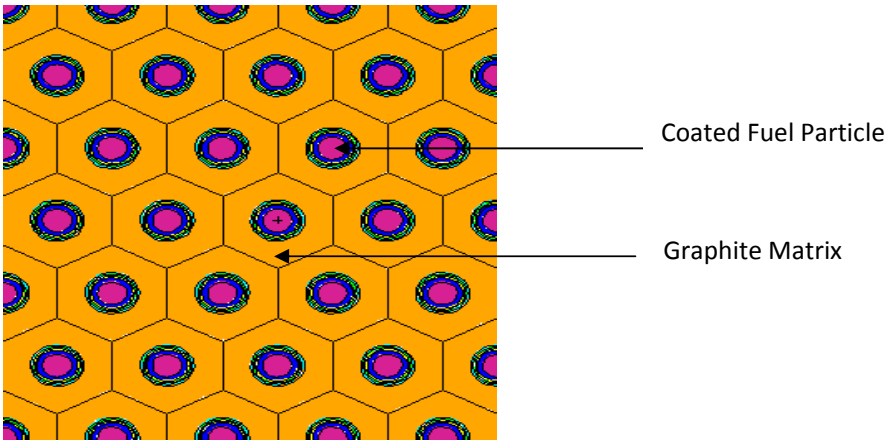

Figure IV.2: MCNP5 model of the CFP's on a triangular lattice.

In modeling a pebble using MCNP5, the CFPs on a triangular lattice are given a universe number. This universe is used to fill the 2.5 cm radius fuel region of the pebble. The fuel region is filled with about 15 000 CFP's embedded in a graphite matrix. The outer non-fuel region of the pebble is modeled explicitly. The model is shown in *Figure IV.3*.

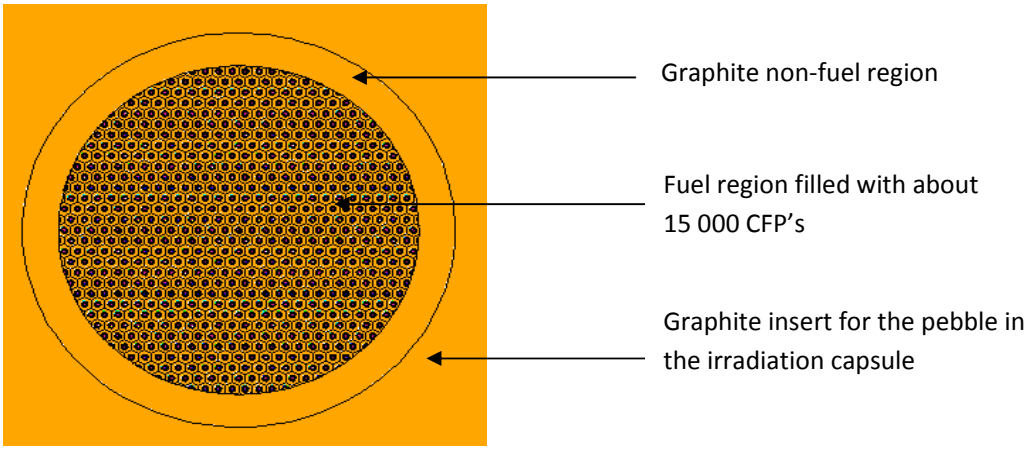

Figure IV.3: MCNP5 model of the pebble.

IV.2.2 Model of an Irradiation Rig

The rig is made of a stainless steel 316L (SS-316L) capsule and contains a 6 cm diameter pebble embedded in graphite, then surrounded by a gas gap filled with helium. *Figure IV.4* represents the engineering drawn of a section of the pebble irradiation rig. This rig is a preliminary design aimed at establishing the know-how of rig design and calculating some neutronic and thermal hydraulic parameters. The final design of the rig will consist of a maximum of about five irradiation capsules each to contain either a pebble or a number of loose CFPs. Again the final rig will be instrumented with thermocouples for temperature measurement and the flux monitors. The final rig design is not yet ready (April 2008), so this dissertation will present results for the preliminary rig design.

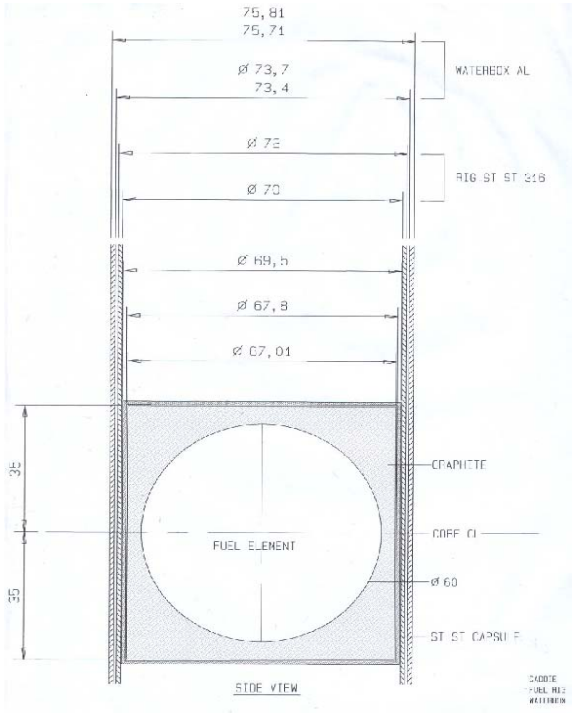

Figure IV.4: The Engineering Drawing of a Section through the Irradiation Rig

The dimensions and material specifications of the rig as well as the material composition of SS-316L are given in *Table IV.1* and *Table IV.2* respectively.

Table IV.1: Dimensions of the PBMR fuel irradiation rig.

Section of the rig	Material	Outer Dimension (diameter) in cm	Material Densities (g/cm^3)
Pebble	6 cm outer diameter sphere described in *Table I.1* and *Figure I.4*		
Graphite	Graphite	6.701	1.74
Gas gap	Helium	6.78	
Capsule	Stainless steel 316L	6.95	7.92
Gas gap	Helium	7.0	
Rig	Stainless steel 316L	7.2	7.92
Water gap	Water	7.34	1.00
Rectangular water box : x and y dimensions respectively in cm			
Water box	Aluminum	7.571 and 7.581	

Table IV.2: Material Composition of Stainless Steel 316L.

Nuclide	Weight Fraction	Atom Density
Iron (Fe)	0.655	0.05594
Chromium (Cr)	0.170	0.01559
Nickel (Ni)	0.120	0.00975
Molybdenum (Mo)	0.025	0.00124
Manganese (Mn)	0.020	0.00174
Silicon (Si)	0.010	0.00170

Figure IV.5 is the MCNP5 model of the preliminary PBMR fuel irradiation rig in the plane parallel to the y-z plane (i.e. the px plane).

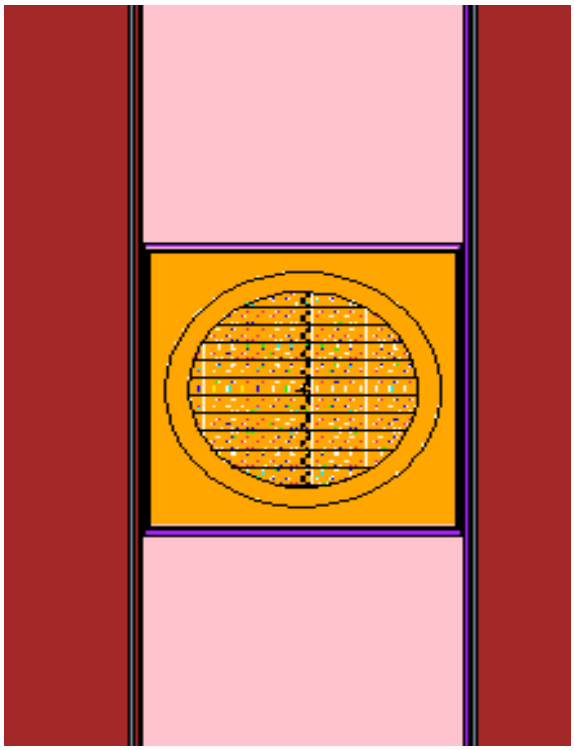

Figure IV.5: MCNP 5 Model of the Pebble Irradiation Rig (z-y section).

IV.2.3 Model of the SAFARI-1 Reactor

A detailed description of the SAFARI-1 reactor is given in chapter II (section II.2.2.2). An MCNP model of the present reactor core was established to calculate the core configurations and to study optimization alternatives. The model describes the fuel assemblies by individual fuel plates and uses 17 axial positions

along the height of the fuel. The six control rods and the molybdenum thimble tubes are also modeled explicitly together with the beryllium reflectors. The OSMINT generated MCNP model of the reactor core is shown in *Figure IV.6*. The vertical cross section of this model is presented to show the axial model of the PBMR fuel irradiation rig in core position B6.

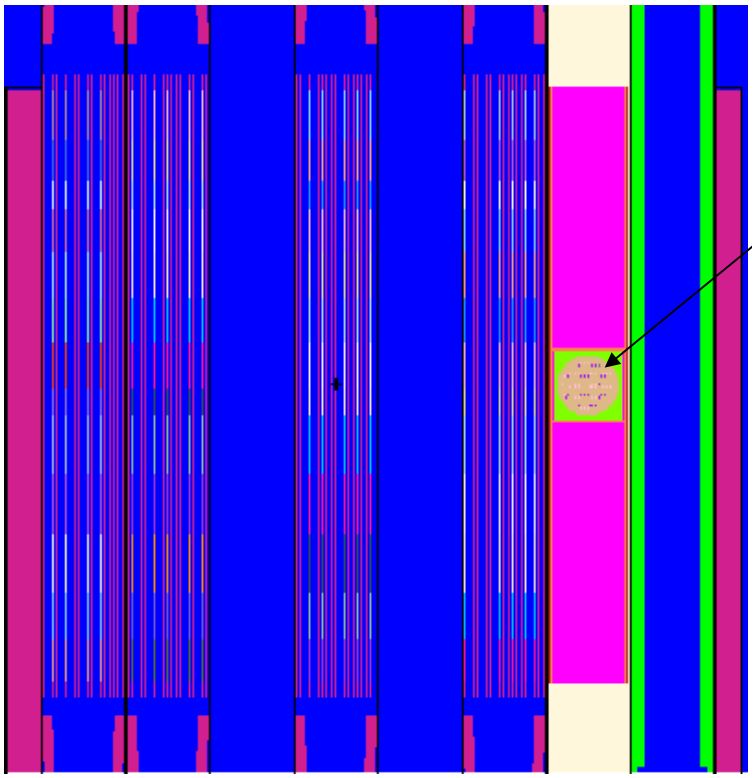

Figure IV.6: Vertical Cross Section of the Core with the Pebble Irradiation Rig in Position B6

IV.3 SIMULATION CALCULATIONS

The irradiation behaviour of the pebble fuel is studied under PBMR simulated conditions in the SAFARI-1 reactor using MCNP5. In an experimental set-up, the high temperature environment in the irradiation rig is obtained by varying the size of the gas gap, varying the ratio of the gas as sometimes a mixture of helium and neon are used as in the HFR and IVV-2M rig or by regulating the gas flow rate. In an MCNP simulation, the high temperature environment is realized through the correct use of high temperature cross sections.

The use the correct temperature dependent cross sections is important in this study. This will help us to determine the effect of Doppler broadening on the fuel absorption resonances and reaction rates. Doppler broadening is a phenomena that occur in the neutron resonance energy region, as the temperature increases, the resonances becomes only broader and more neutrons are absorbed or captured in uranium-238. This means that fewer neutrons will be available to sustain a fission reaction in uranium-235. The Doppler effects adds to the inherent safety features of the fuel hence the high temperature reactors.

For simulation purposes, the following calculations will be performed: reactivity worth calculations, flux distribution calculations and calculations to determine the heating values. The burn-up calculations although described in the next sub-section, they do not form part of this study and will only be a focus for future work.

IV.3.1 Reactivity Worth

It is important from the safety point of view to have knowledge of the reactivity insertion (positive or negative) due to experiments done at any point in time in the reactor core. Reactivity is determined by calculating the multiplication factor of the system. This factor is defined as [47], [51], [52]:

$$k = \frac{\text{number of neutrons in a generation}}{\text{number of neutrons in the preceding generation}} \qquad \text{IV-1}$$

It is described in the so-called "six factor formula" as [47], [51], [52]:

$$k = \eta\, f\, p\, \varepsilon\, P_{FNL}\, P_{TNL} \qquad \text{IV-2}$$

f is the thermal utilization, i.e. the fraction of thermal neutrons absorbed by the fuel compared to the total number of thermal neutrons absorbed in the whole reactor:

$$f = \frac{\Sigma_a^{fuel}\phi_{fuel}}{\Sigma_a^{system}\phi_{system}} \qquad \text{IV-3}$$

ϕ_{fuel} and ϕ_{system} is the average thermal neutron flux in the fuel and the reactor core (system) respectively.

η (eta) is the reproduction factor, the number of fission neutrons produced per thermal neutron absorbed in the fuel

$$\eta = \upsilon\frac{\Sigma_f^{fuel}}{\Sigma_a^{fuel}} = \upsilon\frac{\Sigma_f^{fuel}}{\Sigma_f^{fuel} + \Sigma_{n,\gamma}^{fuel}} \qquad \text{IV-4}$$

υ = average number of neutrons produced per fission

$\Sigma_{\text{f}}^{\text{fuel}}$ = macroscopic fission cross section in the fuel

$\Sigma_{\text{a}}^{\text{fuel}}$ = macroscopic absorption cross section in the fuel

$\Sigma_{\text{n},\gamma}^{\text{fuel}}$ = macroscopic cross section due to other reactions in the fuel

p is the resonance escape probability, i.e. the probability that a neutron will not undergo resonance capture in U-238 while slowing down from the fast to the thermal energy range:

$$p = \frac{\text{number of neutrons leaving the resonance energy range at low energy}}{\text{number of neutrons entering the resonance energy range at high energy}} \qquad \text{IV-5}$$

ε (epsilon) is the fast fission factor, is the factor by which the fast neutron population increases due to fast fissions in U-238

$$\varepsilon = \frac{\text{number of neutrons from thermal fission + number of neutrons from fast fission}}{\text{number of neutrons from thermal fission}} \qquad \text{IV-6}$$

P_{FNL} is the probability that a fast neutron will not leak out of the system and P_{TNL} the probability that a thermal neutron will not leak out of the system. If the product $P_{FNL}P_{TNL}$ in equation IV-2 is equal to unity, which can be the case in very large reactor systems then we obtain the infinite multiplication factor (k-infinity) [47], [51], [52]:

$$\mathrm{k}_{\infty} = \eta\, f\, p\, \varepsilon \qquad \text{IV-7}$$

A system will be critical when the number of neutrons from one generation to the next is equal, i.e. $k = 1$ and the fission chain reaction will continue at a constant power level. Systems go supercritical when the succeeding generation of neutrons results in an increase in number of fissions between the generations, then $k > 1$ and the power level will rise. When succeeding generations of neutrons are causing a decrease in the number of fissions between the generations, then the system is referred to as sub critical, $k < 1$ and the power level decreases [47], [51], [52].

The system multiplication factor $\left(k_{eff}\right)$ or the reactivity $\Delta\rho$ can tell whether the power level in the reactor is constant or whether it increases or decreases. A zero reactivity implies that the power level remains constant; a positive reactivity $\left(+\Delta\rho\right)$ tells that the power level increases and a negative reactivity $\left(-\Delta\rho\right)$ tell that the power level is decreasing. A positive reactivity can be introduced into the system by adding an amount of fissile material (e.g. U-235). The introduction of neutron absorbers in the core leads to negative reactivity insertion. The decrease in the moderator level in the core leads to an increase in neutron leakage, hence introduces a negative reactivity insertion.

In this study, the core k_{eff} will be calculated with and without the irradiation capsule in the core. The reactivity worth or reactivity insertion of the experiment will be determined as:

$$\text{reactivity insertion} = \Delta\rho = k_{eff}\left(\text{experiment in}\right) - k_{eff}\left(\text{experiment out}\right) \qquad \text{IV-8}$$

In MCNP5, the criticality cards facilitate the calculation of multiplication constant through the use of the KCODE source specification and KSRC (source points) entries in the input file. Detailed description of these two entries is given in Chapter III.

IV.3.2 Flux Characterization

It is vital to characterize the radial and axial flux profiles and obtain a quantitative estimate of both the thermal (<0.625 eV) and fast (>1 MeV) flux in the pebble (fuel and non-fuel region), the rig sections, the irradiation position and in the whole core. An accurate knowledge of the fast flux spectrum is important because the fast flux impact on the performance of the fuel (in terms of causing damage on the fuel by knocking of atoms from their equilibrium positions leaving empty interstitial sites that can compromise the integrity of the fuel).

In-core flux measurements can be done by irradiating metal foils ("activation method") because nuclei of certain can be transformed into radioactive isotopes through exposure to neutron radiation. The activity of the radioactive product isotope can then be measured using a counter or detector. The activity is affected amongst other conditions by the neutron flux in the irradiation position and also by the activation cross section of the target material. In foil experiments, the thickness of the target foil is made negligibly small hence imposing the assumption that all the sections of the foil will be irradiated at the same neutron flux. This is ideal since the self shielding effects (lower average neutron flux inside the foil compared to surface due to neutron absorption) are minimized and can be neglected [52], [53].

In a (n,γ) reaction, also known as radiative neutron capture reaction, the target nucleus ${}^{A}_{Z}X$ of atomic number Z and mass number A, absorbs a neutron to form an excited product nucleus $\left({}^{A+1}_{Z}X\right)^{*}$, which de-excites by the emission of a gamma (γ) photon [4]. This reaction is given in the equation below:

$$ {}^{A}_{Z}X + {}^{1}_{0}n \rightarrow \left({}^{A+1}_{Z}X\right)^{*} \rightarrow {}^{A+1}_{Z}X + \gamma \qquad \text{IV-9} $$

The product nucleus may or may not be radioactive. The cross section σ(E) for the (n,γ) reactions are generally higher for thermal than fast neutrons, so that (n,γ) reaction rates are high in a high thermal neutron flux environment such as exists in a reactor such as SAFARI-1 reactor.

During activation in a thermal neutron flux, the reaction rate is expressed as [53]

$$ R = \varphi_{th}\, \sigma_{act}\, N_T \qquad \text{IV-10} $$

ϕ_{th} = thermal neutron flux [$cm^{-2}s^{-1}$]
σ_{act} = microscopic activation cross section [cm^{-2}]
N_T = number of target atoms in the sample

The rate of change in the number of radioactive atoms is the difference between the rates of production and decay [52].

$$\frac{dN(t)}{dt} = \varphi_{th}\,\sigma_{act}\,N_T - \lambda\,N(t) \qquad \text{IV-11}$$

λ = decay constant of the radioactive nuclei produced [s^{-1}]
t = time [s]

At time $t = 0$ (beginning of irradiation), $N(0) = 0$, then solving equation IV-9 using IV-10 gives:

$$N(t) = \frac{R}{\lambda}\left(1 - e^{-\lambda t}\right) \qquad \text{IV-12}$$

If the thermal neutron flux ϕ_{th} is known, then the macroscopic cross section $N_T\,\phi_{th}$ can then be calculated from equation IV-11. This is the cross section of the reaction that leads to the formation of the radioactive nuclide whose activity is measured. The activity of the metal foil at the end of irradiation time T is [52]:

$$A(T) = \lambda N(T) = R(1 - e^{-\lambda t}) \qquad \text{IV-13}$$

Combining equations the latter two equations gives the activity A of the irradiated foil or flux wire, for an irradiation time T and cooling time τ:

$$A(T,\tau) = R\,(1 - e^{-\lambda t})\,e^{-\lambda t} \qquad \text{IV-14}$$

Solving for ϕ_{th}, we get:

$$\phi_{th} = \frac{A(T,\tau)}{N_T\sigma_{act}\left(1 - e^{-\lambda T}\right)\left(e^{-\lambda\tau}\right)} \qquad \text{IV-15}$$

The activity is measured using a calibrated detector set-up. All the other variables such as the N_T, σ_{act}, T and τ are known, so that the flux-rate ϕ_{th} can be determined accurately.

In the SAFARI-1 reactor copper foils are used to characterize the thermal flux while the fast flux is characterized by the nickel foil in the reaction $^{58}Ni(n,p)^{50}Co$ with the cobalt isotope having a half life of 70.82 days. This reaction has an energy threshold at $E = 1\,MeV$. In MCNP5, the flux is calculated using the F4 tally as described Chapter III. This tally can also be modified as described to calculate reaction rates.

IV.3.3 Heating Values

It is also of importance to calculate radial and axial heating profiles in the pebble and the rig. This is fission heating and heating due to prompt and delayed photons. This information will be input into thermal hydraulic calculations to confirm that the correct environment was simulated. In-core calorimetry provides a practical and flexible method to measure heat deposition in order to describe in advance the experimental conditions and environment for the experiments that are to be conducted.

Calorimeter experiments were done in the SAFARI-1 reactor to measure heat deposition in some core positions. In this experiment a calorimeter made of molybdenum (Mo) or stainless steel core is surrounded by a vacuum of air and contained in a stainless steel jacket. The calorimeter is instrumented with two high temperature thermocouples that are connected to a signal detector or monitor, one in the centre of its core and another one in the stainless steel jacket. During insertion of the device in the core, the radiation flux deposits a power P in the core of mass m which causes a rise in the core temperature (θ) hence a heating curve is obtained and upon withdrawal, a cooling curve is obtained [55]. The time rate of power in the device is expressed as the amount of energy deposited=heat rise in the calorimeter core + losses towards the walls:

$$\overline{P}\,dt = m\,C\,d\theta + \frac{\theta - \theta_0}{R}dt \qquad \text{IV-16}$$

C is the specific heat and R the thermal insulation resistance between the core and walls of the calorimeter which are both a function of temperature [54]. When an equilibrium temperature θ_e is reached, $d\theta$ becomes very small and equation IV-15 becomes:

$$P = \frac{\theta_e - \theta_0}{R_e} \qquad \text{IV-17}$$

When the calorimeter is withdrawn from the core, with $P = 0$, then equation IV-15 becomes

$$\frac{d\theta}{dt} = -\frac{\theta - \theta_0}{RmC} \qquad \text{IV-18}$$

At some equilibrium time t, equation IV-17 yields:

$$\left(\frac{d\theta}{dt}\right)_e = -\frac{\theta_e - \theta_0}{R_e m C_e} \qquad \text{IV-19}$$

When the cooling curve is plotted on a semi log scale, $\log(\theta - \theta_e)$ versus time t, then a straight line is obtained. Therefore it is deduced that the equation: $(\theta - \theta_0) = (\theta_e - \theta_0)e^{-t/T_0}$ gives:

$$\left(\frac{d\theta}{dt}\right)_e = -\frac{(\theta_e - \theta_0)}{T_0} \qquad \text{IV-20}$$

Upon combining equations IV-18 and IV-19 we get $T_0 = R_e m C_e$ and then we get fromIV-15 power expressed in watt/gram (W/g):

$$\frac{P}{m} = C_e \frac{(\theta_e - \theta_0)}{T_0} \qquad \text{IV-21}$$

In equation IV-20 above, the temperature difference is measured by the thermocouples (one in the calorimeter core and the other in the jacket/wall), specific heat can be obtained from the literature and the pseudo-period T_0 can be obtained from the graph of $\log(\theta - \theta_e)$ versus time t as the difference in the abscissa of two points [54].

In MCNP, the amount of heat deposited, hence the power distribution levels, is calculated using the F7 tally for fission energy heat track length estimate, and the F6 tally for the total heating track length estimate. Alternatively, the F4 card with the modifier (FM card) can be used as described in Chapter III to obtain answers equivalent to the F6 and F7 tallies.

IV.3.4 Burn-up

It will also be of importance to study the burn-up profile of the pebble. This refers to the depletion of the fissile material in the fuel with time and exposure to some thermal neutron flux. The result of a pebble burn-up study provides information about the time dependent core and fuel composition, thermal power distribution and multiplication factor. A burn-up study falls beyond the scope of this work, it is worth mentioning that high burn-up levels of up to 100 000 MWd/tU) are expected with the HTR fuel.

Burn-up is defined as the measure of the total amount of thermal energy generated per unit quantity of heavy element in the core [51], [52]. This parameter is expressed in units of percentage of heavy element that have undergone fission, MWd/tU – MegaWatt days per ton of uranium for a reactor fuelled with UO_2. In high temperature gas reactors this parameter is usually expressed in the unit of %FIMA (i.e. percentage of "fissions per initial metal atom") where the initial metal atom refers to the total number of uranium atoms for UO_2 fuelled core [52].

In core or fuel depletion studies, the following neutron balance equation is solved:

$$\frac{dN_i}{dt} = \text{formation rate} - \text{destruction rate} - \text{decay rate} \qquad \text{IV-22}$$

The above equation defines the rate at which the concentration of a nuclide N_i (number of nuclei/cm^3) changes with time both during reactor operation and at shutdown. The formation rate is defined as:

$$\text{Formation rate} = \gamma_i N_f \sigma_f \varphi + N_j \sigma_j \varphi + \lambda_k N_k \qquad \text{IV-23}$$

γ_i = fission yield of nuclide i

N_f, N_j, N_k = number densities of the fissile nuclides and nuclide j and k respectively

σ_f = microscopic fission cross section of the fissile nuclide

σ_j = microscopic capture cross section of nuclide j

φ = neutron flux

λ_k = radioactive decay constant of nuclide k

Equations IV-20 and IV-21 below express the destruction and decay rate respectively.

$$\text{Destruction rate} = N_i \sigma_i \varphi \qquad \text{IV-24}$$

$$\text{Decay rate} = \lambda_i N_i \qquad \text{IV-25}$$

Combining equations IV-22, 23 and 24 into IV-21 gives:

$$\frac{dN_i}{dt} = \gamma_i N_f \sigma_f \varphi + N_j \sigma_j \varphi + \lambda_k N_k - N_i \sigma_i \varphi - \lambda_i N_i \qquad \text{IV-26}$$

In order to solve equation IV-26, one needs to have knowledge of the neutron flux spectrum. This entity is dependent on the composition of the fuel, which is dependent on the neutron flux, which in turn depends on the fuel composition. This complicates the process of solving the depletion this equation. This can be resolved by calculating the neutron flux distribution at a time t using group-diffusion method at a known core composition and assuming the flux to remain constant in a time interval Δt with the reactor in operation. The composition of the system at a time $t + \Delta t$ can then be calculated. This process is then iterated for each different time step calculating the new neutron flux distribution at each step [51], [52].

The effort of doing depletion studies can also be reduced by reducing the number of nuclides to be studied in the chain reaction IV-22. Nuclides with very large cross sections are considered as more important and these are xenon-135 and samarium- 149. The rest of the nuclides are lumped together and assigned a single average cross section. Another approach is to reduce the number of heavy nuclides included in the calculations. Any nuclide with a very short half life can be omitted. Nuclides of most importance are uranium-235, -236, and -238 as well as plutonium-239, -240, -241 and sometimes -242 and other actinides [52].

Computer code systems are available to perform depletion studies. These codes include ORIGEN developed at Oak Ridge National Laboratory. Accuracy is enhanced by coupling transport codes to these depletion codes to perform burn-up calculations. Amongst these coupled codes, there is MONTEBURNS which couples MCNP and ORIGEN.

CHAPTER V : RESULTS AND DISCUSSION

V.1 CHARACTERISATION OF THE SAFARI-1 REACTOR CORE

An accurate knowledge of the neutron flux distribution in a reactor core is required for characterization of the core irradiation capabilities. This section presents neutronic characterization of the SAFARI-1 reactor core in terms of:

- Reactivity effects,
- Neutron and photon flux spectrum/distribution
- Power distribution.

The neutronic behavior of the SAFARI-1 core is studied for two defined cases:

- **CASE I (RIG OUT)**: a SAFARI-1 standard core with molybdenum target plates and irradiation channels B6, D6 and F6 filled with water, hence a core model excluding the PBMR fuel irradiation rig in core position B6.
- **CASE II (RIG IN)**: a SAFARI-I standard core with molybdenum target plates, irradiation channel B6 loaded with the PBMR fuel irradiation rig and channels D6 and F6 filled with water.

V.1.1 Reactivity Effects

The reactivity effects on the reactor core due to insertion of the PBMR fuel irradiation rig are studied. In order to determine the reactivity effects, a criticality calculation is performed in MCNP5. A typical input line for such a calculation read as follows:

```
KCODE    1.0e6    1.0    15    215
```

Simply described, the input line is for an eigenvalue calculation in MCNP5, with 1.0×10^{6} number of source histories per cycle with an initial k_{eff} guess of 1.0, skipping 15 cycles before beginning tally accumulation and running for a total of 215 cycles.

All the calculations reported in this chapter, were performed for BoC 0803-1 with molybdenum rigs incorporated in the core. The reactivity effects are calculated for the two cases: RIG OUT and RIG IN as described in section V.1. The results of k_{eff} calculations are presented in *Table V.1*. The reported k_{eff} is the combined collision/absorption/track-length.

Table V.1: Reactivity effects of the PBMR fuel irradiation rig

Scenario	**k_{eff}**	**Reactivity, ρ (pcm)**
a) RIG OUT	1.02274±0.00005	2223
b) RIG IN	1.02226±0.00005	2177

The reactivity (ρ) is calculated as $\rho = \frac{ke_{ff}-1}{k_{eff}}$ in the units of $\frac{\Delta k}{k}$. This unit is further multiplied by a factor of $10^5$to obtain reactivity in the units of percent millirho (pcm). From *Table V.1*, it is noted that the core is more reactive without the rig in core position B6. Further on, a calculation of the reactivity worth of the PBMR fuel irradiation rig, $\Delta\rho = k_{eff}\,(\text{RIG IN}) - k_{eff}\,(\text{RIG OUT})$ reveals that the rig has a negative reactivity worth of 46 pcm. While this is not expected since the rig contains 9g of fissionable UO_2 fuel, which should increase the core reactivity, it is further noted that the rig contains vast amounts of helium. When the rig is loaded in core channel B6, the water moderator in the channel is displaced introducing instead the helium gas. The introduction of helium due the displacement of the water moderator then affects mostly two terms in the k_{eff} equation described in section IV.3.1: the thermal utilization factor and the reproduction factor – in that the fuel pebble will see very little thermal neutrons due to lack of moderation or thermalization in the channel and there will be very few fission multiplicity.

V.1.2 Neutron Flux Distributions in the Reactor Core

V.1.2.1 Neutron Flux Spatial Distribution

The spatial neutron flux distribution in the SAFARI-1 core is calculated using the MESH tally capability of MCNP5. Using this feature, a mesh tally can be superimposed over the problem geometry. Two geometrical MESH types can be handled by the code: rectangular and cylindrical meshes. For the purpose of this study, rectangular meshes are used. Currently the MESH tally in MCNP5 can only be used with the F4 track length tally. The general code input line below shows a typical MCNP5 input line for the calculation of MESH based neutron flux:

```
FC14 total neutron flux in the SAFARI-1 core
FMESH14:n    GEOM = REC    ORIGIN  -34.695    -28.35    -29.685
             IMESH  = 34.695       IINTS = 9
             JMESH  = 36.45        JINTS = 8
             KMESH = 29.685        KINTS = 1
             EMESH =  0.625e-6    5.53e-3    0.821    20
             EINTS  =        1          1         1        1
FM14    1.6467918e18                                    $ tally normalization constant
```

The first line of the code input line is a comment (FC) on the tally number 14-it simply describes tally number **14** for ease of reference and can also be used as a title of the graph for tally plotting purposes. On the second line, FMESH entry invokes a MESH tally number 14 for particle type **n** (a neutron, which can also be a photon or an electron). The mesh geometry (**GEOM**) is rectangular (**REC**) with the x, y and z coordinates of the **ORIGIN** as specified. The location of the coarse meshes in the x, y and z directions is specified by the **IMESH**, **JMESH** and **KMESH** entries respectively. The number of fine meshes within

the corresponding coarse meshes is specified by **IINTS**, **JINTS** and **KINTS** in the x, y and z directions respectively. The **EMESH** card specifies the values of the coarse energy meshes (in MeV) while the **EINTS** card specifies the number of fine meshes within the corresponding coarse energy meshes. The FM card is the tally multiplier card where normalization constants and other multipliers can be input to obtain the tally in the correct units.

The above code input line simply imposes a rectangular MESH tally on the SAFARI-1 reactor core. The coarse MESH: starts from -34.695 in the x-direction and extends to +34.695, it is further divided into nine (9) finer meshes, starts from-28.35 in the y-direction and extends to +36.45 and is further divided into eight (8) finer meshes and starts from -29.685 in the z-direction and extends to +29.685 with just one (1) fine mesh. The energy coarse meshes are the energy bins of interest: from 0-0.625 eV for the thermal energy range, 0.625eV-5.53keV for the resolved resonance region, 5.53keV-0.821 MeV for the unresolved resonance region and 0.821MeV-20MeV for the fast energy region. Each of the energy coarse meshes is divided into just one fine mesh.

*Table V.2: Total assembly averaged neutron fluxes for the SAFARI-1core with RIG IN (**green**) and RIG OUT (**red**) × 10^{14} neutrons/cm^2.s*

	1	2	3	4	5	6	7	8	9
A	**0.650** **0.659**	**1.105** **1.125**	**1.596** **1.637**	**2.012** **2.092**	**2.162** **2.300**	**1.986** **2.162**	**1.655** **1.856**	**1.203** **1.312**	**0.753** **0.802**
B	**0.892** **0.903**	**1.711** **1.733**	**2.727** **2.767**	**3.386** **3.464**	**3.483** **3.498**	**3.725** **3.057**	**2.701** **2.863**	**2.121** **2.244**	**1.293** **1.352**
C	**1.110** **1.117**	**2.180** **2.197**	**3.625** **3.655**	**4.368** **4.409**	**4.421** **4.411**	**4.044** **3.939**	**3.555** **3.600**	**2.799** **2.872**	**1.804** **1.853**
D	**1.274** **1.282**	**2.480** **2.492**	**3.871** **3.892**	**4.814** **4.838**	**5.022** **5.033**	**5.507** **5.516**	**4.057** **4.091**	**3.238** **3.284**	**1.984** **2.019**
E	**1.451** **1.457**	**2.732** **2.737**	**4.164** **4.179**	**4.921** **4.938**	**4.973** **4.987**	**4.732** **4.749**	**4.026** **4.056**	**3.040** **3.071**	**1.860** **1.883**
F	**1.472** **1.476**	**2.719** **2.731**	**3.947** **3.962**	**4.859** **4.872**	**5.052** **5.065**	**5.513** **5.541**	**3.911** **3.936**	**3.121** **3.143**	**1.884** **1.899**
G	**1.304** **1.309**	**2.436** **2.446**	**3.717** **3.727**	**4.426** **4.439**	**4.614** **4.627**	**4.403** **4.422**	**3.669** **3.689**	**2.659** **2.672**	**1.580** **1.586**
H	**0.972** **0.974**	**1.790** **1.796**	**2.666** **2.677**	**3.327** **3.336**	**3.539** **3.553**	**3.374** **3.390**	**2.833** **2.844**	**1.906** **1.912**	**1.055** **1.058**

The results of an MCNP5 calculation of the spatial neutron flux in the SAFARI-1 core are presented in *TABLE V.2* for the scenarios RIG IN and RIG OUT, of which the standard deviation in these results is in the order of 10^{-3}. It is noted from this results that the maximum neutron flux is localized in core position F6, both when a rig is loaded in position B6 and when it is removed. Position F6 is a flux trap position, filled with water for the purpose of this study. The minimum neutron flux is also localized in core position A1 for both cases. The standard deviation for the MCNP5 calculated assembly averaged neutron flux is in the order of 10^{-3}.

The percentage relative difference in core total assembly averaged neutron flux is calculated and presented in *Table V.3*. For this purpose and throughout this section, the percentage relative difference, calculated as:

$$\% \text{ Relative Difference} = \left[\left(\frac{Q_1}{Q_2}\right) - 1\right] \times 100 \qquad \text{V-1}$$

where Q_1=calculation with RIG IN and Q_2=calculation with RIG OUT

Table V.3: Percentage relative difference in the core total assembly averaged neutron flux

	1	2	3	4	5	6	7	8	9
A	1.38	1.81	2.57	3.98	**6.38**	**8.86**	**12.15**	**9.06**	**6.51**
B	1.23	1.29	1.47	2.30	0.43	**-17.93**	6.00	**5.80**	4.56
C	0.63	0.78	**0.83**	0.94	-0.23	-2.60	1.27	2.61	2.72
D	0.63	0.48	0.54	0.50	0.22	**0.16**	0.84	**1.42**	1.76
E	0.41	0.18	**0.36**	0.35	0.28	0.36	0.75	1.02	1.24
F	0.27	0.44	0.38	0.27	0.26	**0.51**	0.64	**0.70**	0.80
G	0.38	0.41	**0.27**	0.29	0.28	0.43	0.55	0.49	0.38
H	0.21	0.34	0.41	0.27	0.40	0.47	0.39	0.31	0.28

Table V.3 shows that the insertion of a rig in core position B6 leads to a notable 18% reduction in the total assembly averaged neutron flux. The flux depression is mainly attributed to the displacement of the water moderator when the rig is loaded. To a lesser extent, the flux reduction when the rig is loaded can be due to absorption of neutrons in the fuel region of the pebble fuel to cause fission.

Studying the neutron flux pattern in the core positions surrounding B6, *Table V.3* reveals about 6%, 9% and 12% increase in the neutron flux at core positions A5, A6 and A7 respectively with the loading of the rig. Another 6% increase in the neutron flux value is noted in core position B7. Core positions B5 and C5 shows less than 1% change in the neutron flux values while the neutron flux in position C6 is decreased

by up to 3%. In the flux trap positions D6 and F6 and F8, a variation of less than 1% in the neutron flux is calculated when the rig is loaded in core position B6, relative to when it is unloaded.

V.1.2.2 Energy Dependent Neutron Flux

In order to obtain the energy dependent neutron flux spectrum in the core, the following input line in the MCNP5 code is used:

```
FC24 Energy dependent neutron flux in the SAFARI-1 core
F24:n 3
E24 1e-8  1e-7  0.625e-6  1e-5  1e-4  1e-3  5.53e-3  1e-2  1e-1  0.821  1  18i  20
FM24 1.6467918e18
```

The FC card and the FM cards are the same as described in section V.1.2.1. The second line of the input line describes the track length estimate (tally number 24) of neutron (particle designator n) flux in cell number 3 (which is the core). The energy bins are input on the third line in order of increasing magnitude and units of MeV. The third input line also requires for the neutron flux to be calculated in increments of 1MeV between 1 and 20 MeV. Fine energy bins might be required to obtain a better picture of the core neutron flux spectrum.

The average energy dependent neutron flux distribution in the SAFARI-1 core is presented in *Figure V.1*. From this, an initial decrease of less than 1% in the neutron flux is observed in the thermal energy region. This is mainly due to less neutron thermalization in the core as a result of the displacement of the water moderator in core position B6 due to rig insertion. This can also be a result of absorption of thermal neutrons in the fuel region of the pebble during the fission process.

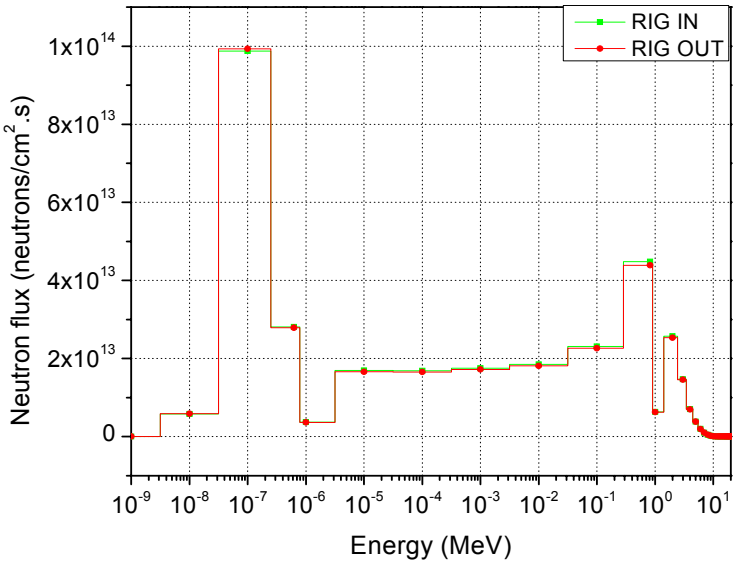

*Figure V.1: Neutron flux in SAFARI-1 for the core with RIG IN (**green**) and RIG OUT (**red**)*

Figure V.1 further reveals that a subsequent 2% increase in the neutron flux is observed in the epithermal energy range. The neutron flux in the fast energy range is increased by about 2% when this rig is inserted. This increase can be attributed to the contribution from the fast neutron emission of the fuel pebble and mainly due to the displacement of the water moderator by the rig. The amount of U-238 introduced by the insertion of this rig is insignificantly small to influence the thermalization process in the whole core, although this effect will be studied once the core is loaded with a rig containing more than one fuel pebble.

The above representation of the neutron flux is not sufficient to describe the global effect of insertion of the PBMR fuel irradiation rig in the SAFARI-1 core. It is therefore imperative to provide some more information on specific energy groups of importance to analysis of the core and its irradiation capabilities. For this purpose and for the context of this work, four neutron energy boundaries were identified: thermal (0-0.625 eV), resolved resonances (0.625eV-5.53 keV), unresolved resonances (5.53keV-0.821 MeV) and fast (0.821 MeV-20 MeV).

A typical MCNP5 to impose the above defined energy bin requirement will be as follows:

```
FC24 Energy dependent neutron flux in the SAFARI-1 core
F24:n 3                                  $ track-length estimate of neutron flux in cell 3 (core)
E24    0.625e-6  5.53e-3  0.821  20      $ energy bins in MeV
FM24  1.6467918e18                       $ tally multiplier to obtain the flux in the desired units
```

The results of the MCNP5 calculation for energy bin averaged neutron flux are reported in *Table V.4*. It is noted from these results that the insertion of the rig in position B6 of the core leads to depression of the total core thermal neutron flux by about 0.4%. The neutron flux is increased by up to 2% in the resolved and unresolved resonance energy regions with the insertion of the rig in core position B6. The overall effect is the increase in the core total neutron flux by about 1% with insertion of the rig.

Table V.4: Energy dependent total core neutron fluxes

	Neutron Flux (n/cm^2.s x10^{14})				
	Thermal neutron region	Resolved resonance region	Unresolved resonance region	Fast neutron region	Total
RIG IN	0.456	0.236	0.250	0.212	1.154
RIG OUT	0.458	0.231	0.245	0.209	1.143
% Relative error	-0.44	2.16	2.04	1.44	0.96

The ratio of the thermal-to-fast neutron flux is another parameter of importance that is used to characterize the core and its irradiation capabilities. From *TABLE V.4*, it is calculated that this ratio amounts to 1.8 and 2.2 respectively for RIG IN and RIG OUT cases.

V.1.3 Photon Flux Distribution in the Reactor Core

V.1.3.1 Photon Flux Spatial Distribution

The photon flux spatial distribution in the SAFARI-1 core is calculated using MCNP5 using the same MESH based philosophy as for the calculation of spatial neutron flux distribution in section V.1.2.1. The difference being to change the tally number and the particle designator on the MESH card from FMESH14:n (neutron) to FMESH114:p (for photons).

The photon flux spatial distribution in the SAFARI-1 core is presented in Table V.5. The standard deviation in these results is in the order of 10^{-3}. The maximum photon flux is in position E5 both for RIG IN and RIG OUT cases. The assemblies at the center of the core shows large photon flux values while reflector positions shows low photon fluxes. The photon flux at the eight positions surrounding B6 all decreases with insertion of the rig. The standard deviation for the MCNP5 calculated assembly averaged photon flux is in the order of 10^{-3}.

Table V.5: *Total assembly averaged photon fluxes for the SAFARI-1 core with a RIG IN (**green**) and RIG OUT (**red**) × 10^{14} photons/cm^2.s*

	1	2	3	4	5	6	7	8	9
A	**1.050** **1.058**	**2.137** **2.153**	**2.898** **2.910**	**3.769** **3.737**	**4.296** **4.089**	**4.102** **3.694**	**3.536** **3.375**	**2.526** **2.500**	**1.378** **1.387**
B	**1.466** **1.470**	**3.150** **3.169**	**5.276** **5.318**	**6.874** **6.912**	**7.250** **6.900**	**6.181** **4.953**	**5.854** **5.656**	**3.854** **3.886**	**2.477** **2.501**
C	**1.789** **1.796**	**3.886** **3.904**	**6.305** **6.334**	**9.039** **9.053**	**9.067** **8.910**	**7.053** **6.741**	**7.427** **7.352**	**5.733** **5.803**	**3.303** **3.336**
D	**1.718** **1.727**	**4.245** **4.262**	**7.505** **7.528**	**10.012** **10.029**	**10.455** **10.435**	**9.673** **9.645**	**8.880** **8.905**	**6.000** **6.044**	**3.547** **3.578**
E	**0.319** **0.320**	**4.030** **4.051**	**7.173** **7.192**	**10.147** **10.180**	**10.622** **10.641**	**10.305** **10.326**	**8.562** **8.613**	**6.416** **6.469**	**3.140** **3.166**
F	**0.275** **0.276**	**3.878** **3.892**	**7.571** **7.590**	**9.963** **9.995**	**10.543** **10.566**	**9.748** **9.776**	**6.767** **6.800**	**5.480** **5.519**	**3.368** **3.388**
G	**0.246** **0.246**	**3.405** **3.414**	**6.327** **6.336**	**9.239** **9.258**	**9.569** **9.599**	**9.312** **9.348**	**7.494** **7.532**	**5.469** **5.501**	**2.942** **2.959**
H	**0.208** **0.208**	**2.725** **2.734**	**5.318** **5.333**	**7.050** **7.069**	**7.573** **7.600**	**7.252** **7.288**	**5.947** **5.976**	**3.891** **3.913**	**1.994** **2.003**

The percentage relative difference in the core total assembly averaged photon flux is presented in Table V.6. Core position B6 shows a 20% photon flux depression when the rig is loaded. Looking at the eight positions surrounding B6, the all show a decrease in the photon flux, with up to 10% decrease in A6 and about 5% decrease in A5, B5 and A7.

Table V.6*: Percentage relative difference in the core total assembly averaged photon flux*

	1	2	3	4	5	6	7	8	9
A	0.76	0.75	0.41	-0.85	-4.82	-9.95	-4.55	-1.03	0.65
B	0.27	0.60	0.80	0.55	-4.83	-19.87	-3.38	0.83	0.97
C	0.39	0.46	0.46	0.15	-1.73	-4.42	-1.01	1.22	1.00
D	0.52	0.40	0.31	0.17	-0.19	-0.29	0.28	0.73	0.87
E	0.31	0.52	0.26	0.33	0.18	0.20	0.60	0.83	0.83
F	0.36	0.36	0.25	0.32	0.22	0.29	0.49	0.71	0.59
G	0.00	0.26	0.14	0.21	0.31	0.39	0.51	0.59	0.58
H	0.00	0.33	0.28	0.27	0.36	0.50	0.49	0.57	0.45

V.1.3.2 Energy Dependent Photon Flux

The same philosophy used for the calculation of the energy dependent neutron flux in the core is adopted for the calculation of the photon flux spectrum. The difference being to change the tally number and the particle designator on the MESH card from FMESH24:n (neutron) to FMESH224:p (for photons). The energy bin card is also modified for photon energies in the energy increments as shown below:

```
FC224 Energy dependent photon flux in the SAFARI-1 core
F224:p 3                                    $ track-length estimate of neutron flux in cell 3 (core)
E224    1e-3 5i 1e-2 5i 1e-1 1 98i 100      $ energy bins in MeV
FM224  1.6467918e18                         $ tally multiplier to obtain the flux in the desired units
```

The photon flux spectrum in the core is also investigated to determine if insertion of the rig leads to any significant perturbation on this spectrum. *Figure V.2* is representative of the core photon flux spectrum. The insertion of the PBMR fuel irradiation rig in core position B6 does not lead to any significant perturbations on the core photon flux spectrum. A large peak is noted in *Figure V.2* at around 1 MeV. This is the energy at which the photons are born from the fission related processes.

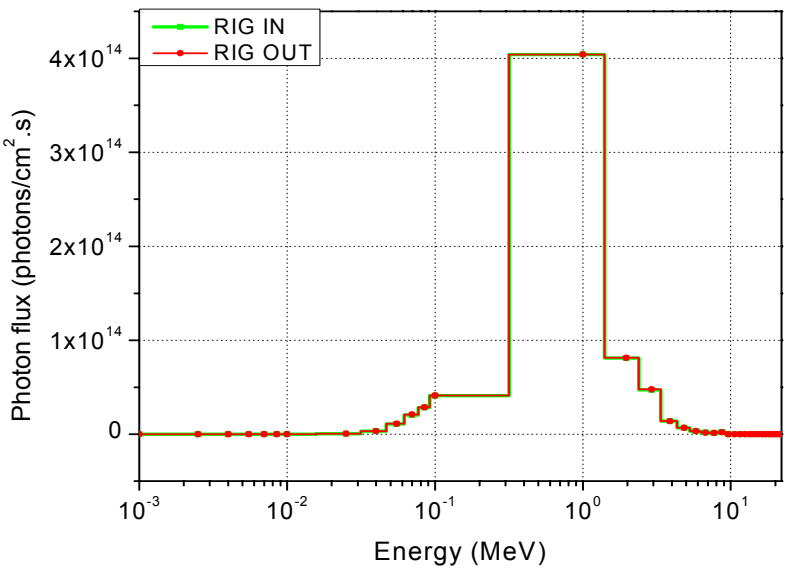

*Figure V.2: Photon flux in SAFARI-1 for the core with RIG IN (**green**) and RIG OUT (**red**)*

V.1.4 Power Distribution in the Core

Determination of power distributions in the core is very important for prediction of temperatures. It is also required for the calculation of the hot channel factor. The power distribution in the SAFARI-1 core is studied to determine whether the insertion of the rig results in a shift in the position where power peaking occurs or any undesirable power peaking.

V.1.4.1 Spatial Fission Power Distribution

The spatial fission power distribution in the SAFARI-1 core is calculated on the same MESH methodology as the spatial neutron and photon flux distribution. The only modification will be in the tally multiplies card (FM) which will read as follows:

```
FM34    -2.6381604636e5    0    -6    8
```

The first entry on the FM card is a constant tally multiplier which is used to obtain the tally in the desired units. The second entry is a zero – so the MESH based tally in MCNP5 does not require a material number for heterogeneous regions-by giving a zero input, the code has a capability to determine the number density for the heterogeneous region. The third entry -6, is the total fission cross section in units of barns while the fourth entry, 8 is the fission Q-value in the units of MeV/collision.

The spatial power distribution in the SAFARI-1 reactor core is shown in *Table V.7*. The standard deviation for the MCNP5 calculated assembly fission power distribution is in the order of $10^{-3}$to 10^{-4}.

It is noted that the hottest channel in the core is localized in position C6. Therefore, the insertion or removal of the rig in position B6 of the core does not lead to a shift in the core hottest channel. The insertion of the pebble irradiation rig, introduces only 0.00293 MW of fission power due to the presence of UO_2 in the kernel of the CFP. This addition is very small to raise concerns with respect to perturbations in the core power distribution.

*Table V.7: Total assembly average fission power distribution in the core (MW) with RIG IN (**green**) and RIG OUT (**red**).*

	1	2	3	4	5	6	7	8	9
A	**0.000** **0.000**	**0.000** **0.000**	**0.000** **0.000**	**0.000** **0.000**	**0.000** **0.000**	**0.000** **0.000**	**0.000** **0.000**	**0.000** **0.000**	**0.000** **0.000**
B	**0.000** **0.000**	**0.000** **0.000**	**0.546** **0.554**	**0.570** **0.585**	**0.664** **0.617**	**0.000** **0.003**	**0.603** **0.591**	**0.065** **0.068**	**0.000** **0.000**
C	**0.000** **0.000**	**0.000** **0.000**	**0.106** **0.106**	**0.683** **0.691**	**0.459** **0.454**	**0.796** **0.734**	**0.418** **0.420**	**0.566** **0.584**	**0.000** **0.000**
D	**0.000** **0.000**	**0.000** **0.000**	**0.644** **0.648**	**0.671** **0.675**	**0.654** **0.656**	**0.000** **0.000**	**0.724** **0.729**	**0.096** **0.097**	**0.000** **0.000**
E	**0.000** **0.000**	**0.000** **0.000**	**0.126** **0.127**	**0.652** **0.654**	**0.476** **0.477**	**0.697** **0.699**	**0.431** **0.434**	**0.581** **0.587**	**0.000** **0.000**
F	**0.000** **0.000**	**0.000** **0.000**	**0.680** **0.681**	**0.604** **0.605**	**0.642** **0.644**	**0.000** **0.000**	**0.707** **0.712**	**0.091** **0.091**	**0.000** **0.000**
G	**0.000** **0.000**	**0.000** **0.000**	**0.109** **0.109**	**0.725** **0.727**	**0.428** **0.429**	**0.629** **0.631**	**0.433** **0.435**	**0.534** **0.536**	**0.000** **0.000**
H	**0.000** **0.000**	**0.000** **0.000**	**0.554** **0.557**	**0.592** **0.594**	**0.624** **0.626**	**0.599** **0.602**	**0.537** **0.539**	**0.000** **0.000**	**0.000** **0.000**

The percentage relative difference in core total assembly averaged fission power distribution is shown in *Table V.8*. A power tilt is observed from the core power distribution map. On the south side of the core, the power decreases in positions B5 by 7%, B7 by about 2%, 1% in C5 and about 8% in C6. This is compensated by collectively small increases on the north side of the core.

Table V.8: Percentage relative difference in the core total assembly averaged fission power distribution

	1	2	3	4	5	6	7	8	9
A	0.00	0.00	0.00	0.00	0.00	0.00	0.00	0.00	0.00
B	0.00	0.00	1.47	2.63	-7.08	0.00	-1.99	4.62	0.00
C	0.00	0.00	0.00	1.17	-1.09	-7.79	0.48	3.18	0.00
D	0.00	0.00	0.62	0.60	0.31	0.00	0.69	1.04	0.00
E	0.00	0.00	0.79	0.31	0.21	0.29	0.70	1.03	0.00
F	0.00	0.00	0.15	0.17	0.31	0.00	0.71	0.00	0.00
G	0.00	0.00	0.00	0.28	0.23	0.32	0.46	0.37	0.00
H	0.00	0.00	0.54	0.34	0.32	0.50	0.37	0.00	0.00

V.1.4.2 Axial Power Distribution in the Core

The axial power distribution in the SAFARI-1 core is calculated the same MESH based approach as described in the calculation of neutron/photon flux spatial distribution and for the fission power distribution, except that the tally multiplier card is modified as follows:

```
FC44 axial  neutron heating in the SAFARI-1 core
FMESH44:n    GEOM = REC    ORIGIN   -34.695    -28.35    -29.685
                IMESH  = 34.695        IINTS = 1
                JMESH  = 36.45         JINTS = 1
                KMESH = 29.685       KINTS = 10
FM44    -2.6381604636e5    0     1   -4
```

The number of finer meshes within the coarse meshes in the x, y and z-directions is modified, so there ten (10) fine meshes in the z-direction and one each in the x and y-directions. Only the third and the fourth entries of this card will be described, as the first two are the same as in the multiplier card for obtaining the fission power distribution in section V.1.4.1. The third entry in this FM card is the total neutron cross section while the fourth entry is the average heating number (MeV/collisions).

The total axial fission, neutron and photon power distribution in the core were investigated. The total axial core power distribution is presented in *Figure V.3* for neutron heating. The total axial neutron heating profile in the core is enhanced by up to 4% in the range spanning the reactor core centerline when the rig is loaded in position B6. The photon and fission axial heating profiles were also calculated and were found to differ by less than 1% with and without the rig in B6.

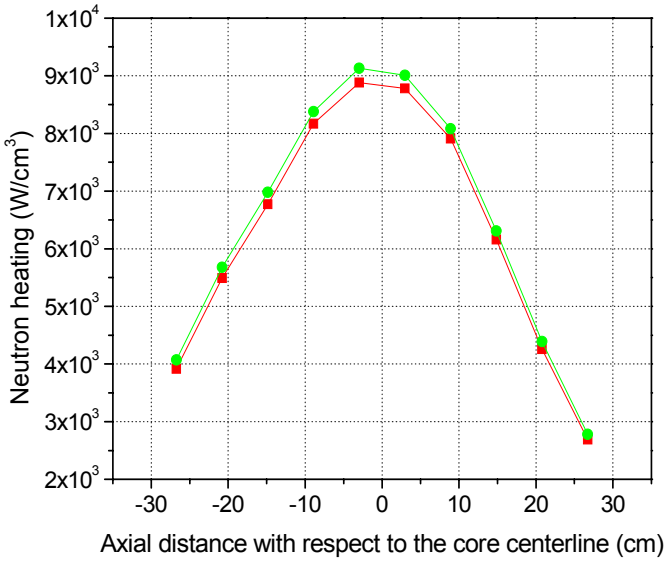

*Figure V.3: Axial neutron heating in the core with RIG IN (**green**) and RIG OUT (**red**)*

V.2 ANALYSIS OF THE B6 IRRADIATION CHANNEL

As it is a requirement to irradiate the PBMR fuel in the SAFARI-1 reactor at a certain neutron flux, for certain duration of time to reach a certain burn-up (according to the client specifications or requirement. Neutronic analysis of core irradiation channel B6 is studied and presented in this section. It is critical for the accurate knowledge of these neutronic parameters to be acquired for the planning of irradiation experiments. Channel B6 is one of the candidate irradiation channels in the SAFARI-1 core for the planned PBMR fuel irradiation experiments. The neutronic parameters of this channel are studied with insertion of the rig (RIG IN) and withdrawal of the rig (RIG OUT) at BoC 0803-1.

V.2.1 Neutron Flux in Irradiation Channel B6

V.2.1.1 Axial Neutron Flux in B6

The axial neutron flux in channel B6 is calculated using the same MESH based methodology as the spatial neutron flux calculation in the core, with the same FM card as for the core calculation, except that the mesh dimensions will be modified to B6 as follows:

```
FC114 total axial neutron flux in channel B6
FMESH114:n     GEOM = REC    ORIGIN   3.855    20.25    -29.685
               IMESH  = 11.565       IINTS = 1
               JMESH  = 28.35        JINTS = 1
               KMESH = 29.685        KINTS = 10
```

The axial profile of the total neutron flux in the in-core irradiation position B6 is presented in *Figure V.4* for the two different core configurations: firstly position B6 is filled with water (RIG OUT) and secondly for position B6 loaded with the pebble irradiation rig (RIG IN). The axial profile is determined by dividing channel B6 into ten mesh points in the axial (z) direction and one mesh point each in the x and y-directions, while using the MCNP5 capability to handle material densities for heterogeneous regions.

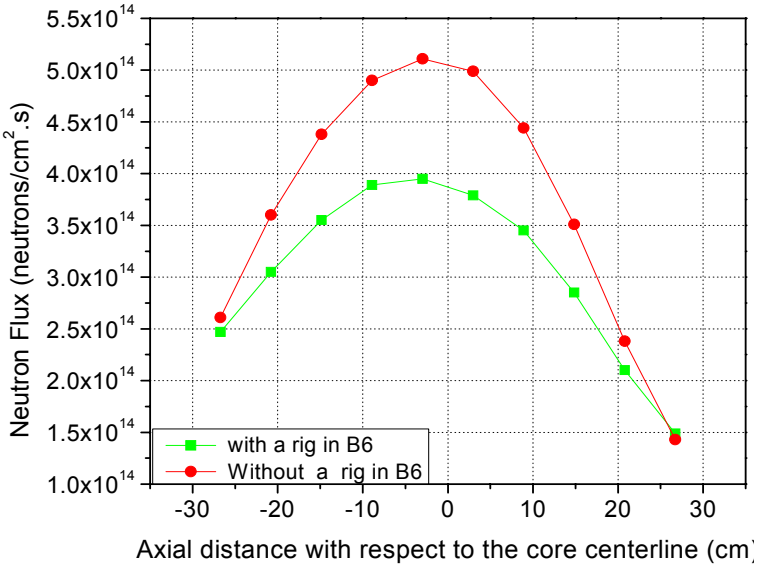

*Figure V.4: Total axial neutron flux in core position B6 for RIG IN (**green**) and RIG OUT (**red**)*

The loading of the pebble irradiation rig in position B6 of the core leads to a 20% depression in the axial neutron flux profile. This is mainly due to the displacement of the water moderator in position B6 by the rig. The other two in-core irradiation positions D6 and F6 only show less than 1% increase in the total axial neutron flux.

V.2.1.2 Energy Dependent Neutron Flux in B6

The energy dependent neutron flux in core position B6 is calculated using the same approach as for the calculation of the energy dependent neutron flux in the reactor core. The energy bins used are the same as for the whole core calculation. Instead of using a cell number to specify core position B6, a lattice element (ijk notation) is used as described below:

```
FC124 Energy dependent neutron flux in channel B6
F124:n   (4<4[1 -3 0])                    $ track-length estimate of neutron flux in a lattice element
FM124  1.6467918e18                       $ tally multiplier to obtain the flux in the desired units
```

The neutron flux energy dependence in channel B6 is presented in *Figure V.5*. A 50% neutron flux depression in the thermal energy range is noticed due to the displacement of the water moderator in position B6 by the rig. Position B6 also shows close to 50% enhancement of the neutron flux in the fast energy range due to the emission of fast fission neutrons from the fuel region of the pebble and reduced moderating effects. The neutron fluxes in the other two in-core irradiation positions (D6 and F6) are slightly perturbed, with an overall increase of less than 1% in the energy dependent neutron flux.

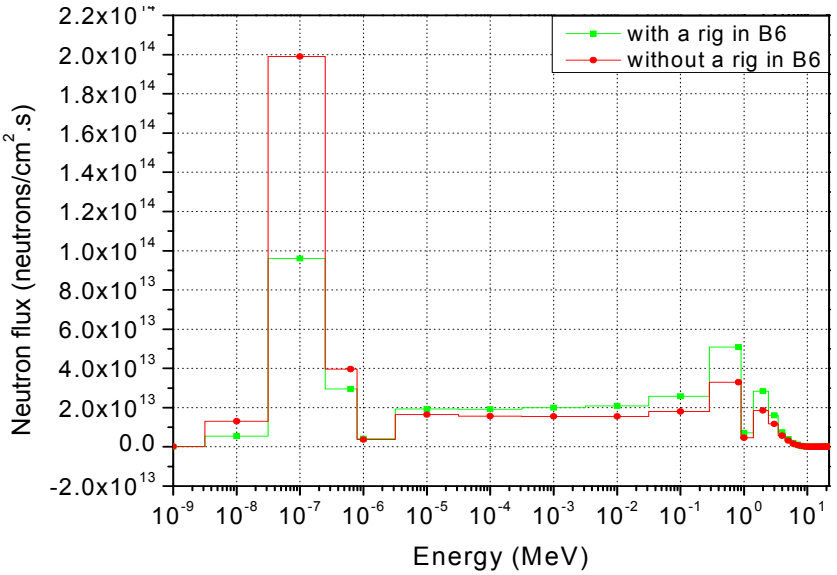

*Figure V.5: Energy dependent neutron flux in irradiation channel B6 with RIG IN (**green**) and RIG OUT (**red**)*

Table V.9 presents the energy dependent neutron flux in core position B6. These are calculated for the four energy groups as defined in section V.1.2.2. The insertion of the rig in core position B6 leads to up to 48% depression in the thermal neutron flux with corresponding increases in the epithermal, resonance and fast energy regions. The overall effect of insertion of the rig in B6 is seen in the reduction of the channel total neutron flux by up to 14%. A calculation of the ratio of thermal-to –fast neutron flux in B6 gives a value of 2.0 for RIG IN compared to 5.4 for RIG OUT.

Table V.9: Neutron flux in irradiation channel B6

	Neutron Flux (n/cm^2.s x10^{14})				
	Thermal	Resolved	Unresolved	Fast	Total
RIG IN	1.310	0.780	0.821	0.668	3.579
RIG OUT	2.516	0.627	0.548	0.469	4.159
% Relative error	-47.93	24.40	49.82	42.43	-13.95

V.2.2 Photon Flux Distribution in B6

V.2.2.1 Axial Photon Flux in B6

The axial photon flux in core position B6 is also calculated in MCNP5 using the same approach as the calculation of the core axial photon flux except modifying the MESH dimensions as done in section V.2.1.1. The axial profile of the total photon flux in the in-core irradiation position B6 is presented in *Figure V.6* for two different core configurations as studied for the neutron flux profile above.

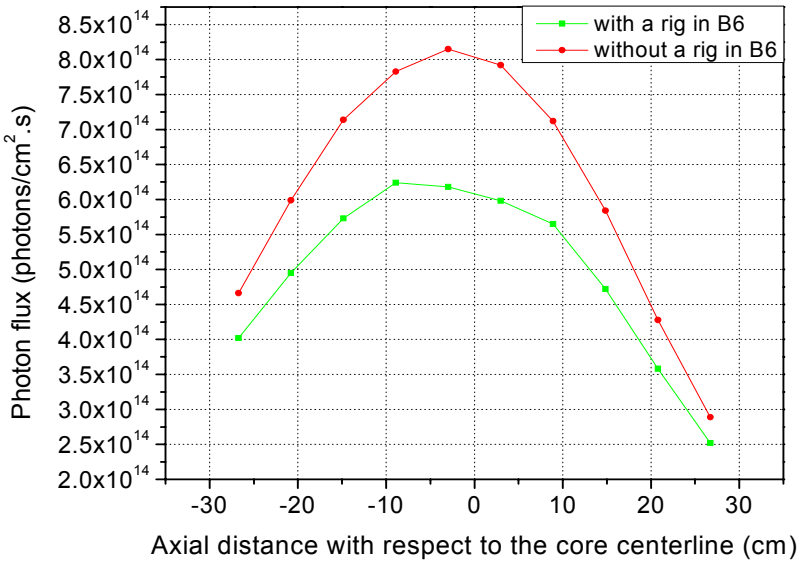

Figure V.6: Total axial photon flux in the core position B6 for RIG IN (Green) and RIG OUT (Red)

The total axial photon flux profile in position B6 is reduced by up to 20% due to the loading of the rig and the absorption of the photons in the rig materials. This effect is more pronounced in the region straddling the core centerline ± 10cm, where there is lots of helium gas and graphite. In position D6, there is a reduction of less than 1% in the photon flux in the region ± 10cm about the core centerline and an increase of 1% in the other regions. Position F6 also shows an overall increase of less than 1% in the axial neutron flux.

V.2.2.2 Energy Dependent Photon Flux in B6

The energy dependent photon flux in core position B6 is calculated using the same approach as for the energy dependent neutron flux. The only difference is to change the particle designator from neutrons to photons and as well to change the neutron energy bins to photon energy bins. In *Figure V.7*, the perturbation on the photon flux profile introduced by loading the rig in core position B6 is more pronounced in the energy range between 0.01 and 10 MeV. A photon flux depression of about 20% is

observed upon insertion of the rig and this can be attributed to the absorption of photons in the rig structures, contributing to nuclear heating in these structures.

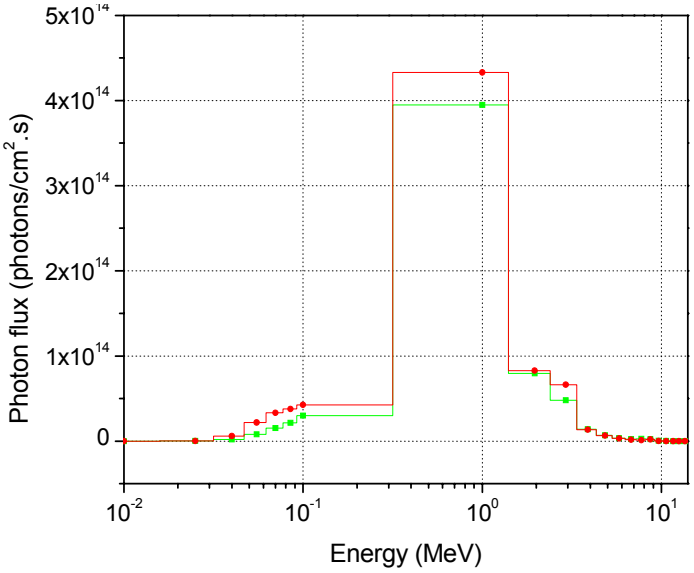

*Figure V.7: Energy dependent photon flux in channel B6 for RIG IN (**green**) and RIG OUT (**red**)*

V.2.3 Power Distribution in Irradiation Channel B6

V.2.3.1 Axial Neutron Heating in B6

The axial neutron heating in core position B6 is calculated using the same methodology as for core axial neutron heating calculations. The only difference being to change the MESH dimensions to the specifications of core position B6.

The axial neutron heating in position B6 of the core is presented in *Figure V.8* for the two core configurations: firstly with position B6 filled with water and secondly loaded with a rig. The standard deviation in these results is in the order of 10^{-3}. The axial neutron power distribution is clearly enhanced in position of B6 of the core due to the introduction of the rig. Neutron heating values were found to increase by one order of magnitude in position B6 where the rig is loaded. This can be attributed to the introduction of materials in B6, the rig and the pebble, with high absorption cross sections for neutrons. Position D6 shows about 1% variation in the neutron heating values in the region ±15 cm about the core centerline and a 2% variation elsewhere. In position F6, a variation of less than 2% in the neutron heating values is observed. The neutron heating values are also enhanced in the regions where water in position B6 is replaced by helium as contained in the rig.

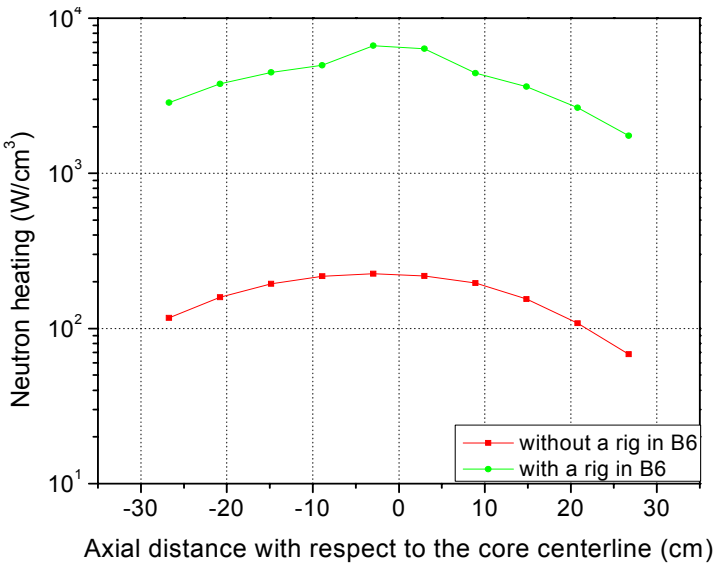

*Figure V.8: Axial neutron heating in irradiation position B6 for RIG IN (**green**) and RIG OUT (**red**)*

V.2.3.2 Axial Photon Heating In B6

Axial photon heating in core channel B6 is calculated in MCNP5 using the same MESH based approach as for the axial neutron flux. The only difference is in the tally multiplier card, which reads:

```
FM34    -2.6381604636e5    0    -5    -6
```

The first two cards are already described as for fission power distribution and axial neutron heating. The third entry, -5 is the total photon production cross section in units of barns and the fourth entry -6 is the photon heating number in units of MeV/collision.

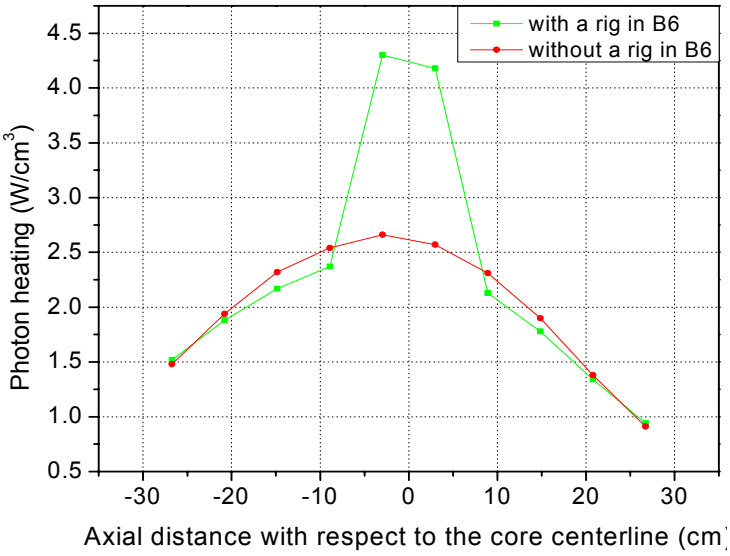

*FIGURE V.9: AXIAL photon heating in the irradiation position B6 for RIG IN (**green**) and RIG OUT (**red**)*

FIGURE V.9 represents the total axial photon power distribution in position B6. The standard deviation in these results is in the order of 10^{-3}. A 60% increase in the photon axial power distribution is observed and more pronounced in the region ±3 cm about the core centerline, with perturbations of less than 10% elsewhere. The increase in the photon heating values in B6 around the core centerline is mainly due to the loading of the rig with materials that have high absorption cross sections for photons as well as photon production in the fuel region of the pebble following the fission process. The overall perturbation in the photon axial heating profiles is less than 1% in position D6 and F6.

The fuel pebble is expected to be irradiated at high temperatures. In order to achieve that, the pebble is placed in a graphite half-cup, surrounded by helium gas contained in a stainless steel rig. The increased gamma heating in the region of the pebble as shown in *FIGURE V.9*, makes it feasible that high temperature pebble irradiation environment can be achieved but this can only be confirmed as final after a thermal hydraulic analysis.

V.3 ANALYSIS OF THE PBMR FUEL IRRADIATION RIG AND THE PEBBLE FUEL

Neutronic parameters were calculated in the different regions of the rig. These parameters include the neutron flux in all the different regions, as well the nuclear heating values. The nuclear heating values will aid the effort of rig design from the thermal hydraulic point of view. Using the MCNP5 calculated nuclear heating values in a thermal hydraulic and heat transfer codes or calculations can help predict and/or confirm the rig operating temperatures.

V.3.1 Neutron and Photon Fluxes in the Rig Regions

The calculation of neutron and photon fluxes in the different regions of the PBMR fuel irradiation rig is performed using the track length estimate of the flux in a cell (F4 tally). A typical input line is shown below:

```
FC134 neutron flux in the rig and pebble regions
F134:n    870  871  872  883  884  885  886  891  892  893  894  895  896
FM134     1.6467918e18
SD134       1    1    1    1    1    1    1    1    1    1    1    1    1
```

The second line of this input describes the track length estimate of the neutron flux in thirteen cells that makes up the rig. The fourth line is the segment divisor card, which is very helpful because sometimes the code cannot calculate volumes of some cells, so the user has to input those volumes. When an SD card is used, the code will divide the tally by the entry on the card. The photon flux in the different regions of the rig is also calculated using the same principles, except that the particle designator has to be changed for photons (p instead of n) and the energy bins has to be modified to photon energies. The neutron and

photon fluxes in the different regions of the PBMR fuel irradiation rig are presented in *Table V.10*. The standard deviation in these results is in the order of 10^{-3}.

Table V.10: neutron and photon flux in the different regions of the PBMR fuel irradiation rig

Description (cell number)	Total neutron flux (n/cm^2.s)	Total photon flux (p/cm^2.s)
Graphite cup (872)	3.835E+14	5.923E+14
Helium gas loop (884)	5.069E+14	7.749E+14
SS316 capsule (885)	5.091E+14	7.711E+14
Helium gas loop (886)	2.899E+14	4.664E+14
SS 316 rig (892)	3.013E+14	4.796E+14
Water channel (893)	3.041E+14	4.960E+14
Aluminum water box (894)	3.072E+14	5.140E+14

The largest neutron fluxes are observed in the SS316 capsule and the first helium gas gap, correspondingly, the largest photon fluxes are also noted in the two regions. The lowest neutron and photon fluxes are noted in the second helium gas loop.

V.3.2 Nuclear Heating in the Rig Regions

The amount of nuclear heating in the different regions of the PBMR fuel irradiation rig is calculated using the F6 tally, that can be used for both neutron heating (F6:n), photon heating (F16:p). The standard deviation in these results is in the order of 10^{-3}.

Table V.11: Neutron and photon heating in the different regions of the PBMR fuel irradiation rig

Description (cell number)	Total neutron heating F16:n (W/g)	Total photon flux F16:p (W/g)
Graphite cup (872)	0.461	1.925
Helium gas loop (884)	6.075	2.574
SS316 capsule (885)	0.041	3.345
Helium gas loop (886)	3.373	1.533
SS 316 rig (892)	0.024	2.076
Water channel (893)	2.897	1.821
Aluminum water box (894)	0.098	2.045

The amount of neutron and photon heating in some regions of the PBMR fuel irradiation rig is found to have a direct proportion relationship with the magnitude of the neutron and photon flux in those regions.

The amount of neutron heating in the rig regions is generally low compared to photon heating except for the neutron heating dominating photon heating in the helium regions of the rig despite the high total photon flux in this region. This is mainly due to the heating of the helium heat transfer medium in the rig by the high energy neutrons (neutrons in the fast energy regime). In the SS316 rig structures, photon heating is found to significantly dominate neutron heating, in the same manner that the photon flux dominates the neutron flux. Nuclear heating of the aluminum structures of the water box and the graphite structures of the rig is also found to be dominated by photon heating.

V.3.3 Nuclear Heating in the Pebble Fuel

The neutron, photon and fission power in the fuel region of the pebble were also calculated and the results are presented in *Table V.12* with the standard deviation in these results is in the order of 10^{-3}. The amount of fission heating in the fuel pebble is found to be the dominate photon heating.

Table V.12: Nuclear heating in the fuel region of the pebble

Pebble power (W)	
Fission	Photon
3803	119

CHAPTER VI : CONCLUSIONS

This study focused on the simulation of the irradiation behavior of the PBMR fuel in the SAFARI-1 reactor. The study entailed development of geometrical models for the PBMR fuel irradiation rig as well as the pebble fuel using MCNP5. The study also entailed investigation of the global effects (whole core) as well as local effects (in core position B6) due to rig. The core neutronic parameters that were investigated are: the reactivity effects of the rig, the neutron/photon flux spatial distribution, neutron/photon flux energy dependence, power distribution and nuclear heating values. Further on, the study focused on calculation of some neutronic parameters in the rig that will aid the improvement of the current design and/or help establish if this rig, loaded in the SAFARI-1 core, can deliver to the expected performance in terms of high temperature irradiation environment.

Models for the preliminary PBMR fuel irradiation rig, the pebble fuel and the coated fuel particles were developed using MCNP5. These models were coupled to an OSMINT generated model of the core for calculation purpose. Reactivity analyses were performed, to determine the reactivity worth of this rig where upon calculations revealed that the insertion of this rig in core position B6 lowers the reactivity of the core. The reactivity worth of the rig is calculated and amounts to 46 pcm. The lowered reactivity is mainly due to less thermalization of neutrons in the core, due to the displacement of the water moderator in channel B6 by the rig, subsequently introducing vast amounts of helium in the channel.

Despite the loading of the rig in core position B6, the core hottest spot still remain localized in core position C6. The insertion of the rig in core position B6 leads to a power tilt on the south side of the core, with decreased assembly averaged fission power. This effect is compensated by correspondingly small increases in the assembly averaged fission power on the north side of the core. The rig is found to add up only 0.00293 MW of fission power in the core due the presence of the UO_2 fuel kernels in the coated fuel particles of the pebble. This addition is of course very small to raise any concerns with respect to perturbations on the core power distribution. The nuclear heating values in the core are not significantly perturbed by the insertion of the rig, the relative differences of up to 4% were observed for axial neutron heating in the core for RIG IN and RIG OUT cases.

The preliminary rig design used in this study contains just one fuel pebble and is found to have insignificant effect on the core neutron and photon flux spectrum. The relative differences in the magnitudes of these parameters for RIG IN and RIG OUT were found to be less than 1% in most of the core assemblies. The eight core positions surrounding B6 were the most affected as a result of the loading of this rig. The magnitudes of the energy dependent neutron and photon flux in the core were also found to be perturbed to no more than 2% due to rig insertion. Therefore, the insertion of this rig in core position B6 does not lead to any softening or hardening of the core neutron/photon flux spectrum.

The influence of the loading of this rig on the magnitude of the neutron and photon flux in core position B6 are more pronounced. The magnitude of the neutron flux is depressed by up to 18%, while the magnitude of the photon flux is reduced by up to 20% when the rig is loaded. These effects are mainly attributed to the displacement of the water moderator in channel B6 and the introduction of vast amounts of helium in channel B6 due to rig insertion, which lead to less neutron thermalization.

In core position B6, the axial neutron heating values were increased by one order of magnitude when the rig is loaded. The axial photon heating values in core position B6, in the region spanning ± 10cm with respect to the core centerline were increased by up to 60% due the loading of the rig. This may imply that more photon heat is absorbed by the rig structural materials in that region. Therefore a direct proportion relationship is noted between the magnitudes of the neutron/photon flux and the neutron/photon heating values. In core position B6, the reduced magnitudes of the neutron and photon fluxes converts into increased nuclear heating values. In the structural regions of the rig, photon heating dominates neutron, except in the helium gas loops where the reverse is true.

The preliminary design of the PBMR fuel irradiation rig used in this study does not pose any significant concerns on isotope and other material irradiations. The neutron flux in the eight molybdenum production site is found to rather increase by a factor of less than 1% when the rig is loaded in core position B6 except for core position B8 experiencing an increased neutron flux of about 6%.

Pre-irradiation analyses of the preliminary PBMR fuel irradiation rig reveals promising performance characteristics of this rig, in terms of increased neutron/photon heating in the rig structures. This gives hope, pending heat transfer and thermal hydraulic calculations, that the envisaged high temperature irradiation of the pebble fuel in the SAFARI-1 reactor core can be achieved.

CHAPTER VII : RECOMMENDATIONS FOR FUTURE WORK

The PBMR fuel irradiation rig used in this study is a preliminary design, containing just one fuel pebble in core channel B6, located symmetrically along the core midplane. In future this rig will be extended to contain about four or five fuel pebbles. The effect of this rig on the core neutronic parameters will then need to be re-investigated.

An accurate method for the calculation of nuclear heating in the core, the rig and its structural materials has to be investigated. Currently, MCNP5 can only calculate neutron and prompt gamma heating. The effect of delayed gammas has to be taken into account. In future, ORIGEN calculations will be performed to properly account for delayed gammas.

For the purpose of this study, material cross sections for the whole core, including the rig and the pebble fuel were evaluated at about 300K, using the ENDF-VI.8 cross section file and in some cases the ENDL libraries. Since it is a requirement to design a rig that will be capable of exposing the PBMR fuel to the high temperature environment typical to that of the PBMR, future studies will need to focus on adjusting the material cross sections in the different regions of the rig to this expected high temperatures. The use of high temperature fuel cross sections will then be investigated to account for Doppler effects in the fuel.

The use of variance reduction techniques in MCNP5 to obtain better tally statistics will also be investigated. When tallying is done in very small regions of the core, in a whole core calculation, the number of neutron tracks entering such small regions in space is found to be very small and that affects the reliability of the results. So, the variance reduction techniques will aim at increasing the importance of the cells or regions of interest in the geometry and as well help to drive more particles towards those regions.

Also to be investigated in future, is the impact of the planned PBMR fuel irradiation experiments on the SAFARI-1 core operational schedule, in terms of the core cycle length, isotope production and its irradiation capabilities for other materials.

REFERENCES

[1] S. Ion, *et al*. Pebble Bed Modular Reactor. *The First Generation IV Reactor to be Constructed*. World Nuclear Association Annual Symposium, 3-5 September 2003, London.

[2] J. Slabber. *Pebble Fuel Advantages*. 2nd International Topical Meeting on High Temperature Reactor Technology. Beijing, China. September 22 – 24 2004.

[3] D. Nicholls. *The Pebble Bed Modular Reactor, Desalination Challenges and Options*. Int. J. Nuclear Desalination, Vol.1, No.4, 2005.

[4] T. Dudley, P. de Villiers, W. Bouwer, R. Luh. *The Operator Training Simulator System for the Pebble Bed Modular Reactor (PBMR) Plant*. Nuclear Engineering and Design 238 (2008) 2908-2915

[5] P.J. Venter, M. N. Mitchell, F. Fortier. *PBMR Reactor Design and Development*. 18th International Conference on Structural Mechanics in Reactor Technology (SMiRT18), Beijing, China, August 7-12, 2005.

[6] N. Kemp. *Basic Principles of PBMR Operations and Control*. 8 November 2002. https://odin.jrc.nl/htr-tn/HTR-Eurocourse-2002/Kemp_580.pdf

[7] http://www.pbmr.co.za

[8] D. Matzner. *PBMR Existing and Future R & D Facilities*. 2nd International Topical Meeting on High Temperature Reactor Technology. Beijing, China. September 22 – 24, 2004.

[9] M. Koch. *Preliminary Modeling of PBMR Kernel Irradiation in SAFARI-1*. RRT-PBMR-06-01

[10] *Development Plan for Advanced High Temperature Coated-Particle Fuels*. Issued by General Atomics for the Department of Energy. Contract No. DE-AC03-01SF22343, Document Number PC-000513, Revision 0.

[11] K. Kugeler. *Reactor Safety Handbook*. Reactor Safety Course presented at the University of the NorthWest (Potchefstroom) for M.Sc. Nuclear Engineering, 2005.

[12] R. Prinsloo, D. Naidoo and F. Reitsma. *Oscar-3 Workshop*. February 2003.

[13] X-5 Monte Carlo Team. MCNP-*A General Monte Carlo N-Particle Transport Code*, Version 5. Volume I: Overview and Theory. April 24, 2003.

[14] M. Belal, A. Graham, B.M Baloi. *OSMINT Verification and Validation*. November 2006. Necsa, Radiation and reactor Theory Internal Report No. RRT-FMR-REP-09005, Revised August 2009

[15] H. Nabielek, W. Kuhnlein, W. Schenk. *Development of Advanced HTR Fuel Elements*. Nuclear Engineering and design 121 (1990) 199-210

[16] W. von Lensa. *Former HTR Concepts and Large Experimental Facilities*.HTR/ECS Cadarache, France, November 4-8, 2002.

[17] T. Abram. *Pebble Bed Modular Reactor: Technology and Project Overview*. Presentation attached in Appendix C

[18] A. C. Kadak. *High Temperature Gas Reactors the Next Generation?* Argonne National Laboratory, July 14, 2004. http://web.mit.edu/pebble-bed/Presentation/HTGRnextgen.pdf

[19] IAEA TECDOC 1198. Current Status and Future Development of Modular High Temperature Gas Cooled Reactor Technology, IAEA, Vienna, Austria

[20] IAEA TECDOC 1238. IAEA Technical Committee Meeting on "Gas Turbine Power Conversion Systems for Modular HTGRs", Palo Alto, California, 14-16 November 2000

[21] S. S. Penner, R. Seiser, K. Schultz. *Nuclear Energy for the future*. http://www.ddponline.org/penner05.pdf

[22] G. C. Bramblett, C. R. Fisher, F. E. Swart. *Operational Experience at Fort St. Vrain*. IAEA International Working Group on Gas Cooled Reactor (IWGCR) Safety and Licensing Aspects, Lausanne Switzerland, 1-3 September 1980. IWGCR-1, pp 6-10

[23] H. Nickel. *HTR Coated Particles and Fuel Elements*. HTR EUROCOURSE 2002, CEA Cadarache/France.

[24] M. P. Labar. *The Gas Turbine-Modular Helium Reactor: A Promising Option for Near Term Deployment*. GA-A23952.

[25] D. A. Petti *et.al*. *Key Differences in the Fabrication of US and German TRISO-Coated Particle Fuel and their Implications on Fuel Performance.* 2nd International Topical Meeting on High Temperature Reactor Technology, Petten, Netherland, 22-24 April, 2002

[26] K. Bakker *et.al*. *Status of Facilities and Experience for Irradiation of LWR and V/HTR Fuel in the HFR Petten*. Proceedings of the International Symposium on Research Reactor and Neutron Science-In Commemoration of the 10th Anniversary of HANARO-Daejon, Korea, April 2005.

[27] A. W. Mehner *et.al*. *Spherical Fuel Elements for Advanced HTR Manufacture and Qualification by Irradiation Testing*. Journal of Nuclear Materials 171 (1990), 9-18.

[28] H. Huschka *et.al*. *Fuel for Pebble Bed HTRs*. Nuclear Engineering and Design 78 (1984) 155-166.

[29] J. Ahlf *et.al*. *Irradiation Experiments on High Temperature Gas-Cooled Reactor Fuels and Graphites at the High Flux Reactor Petten*. Journal of Nuclear Materials 171 (1990) 31-36.

[30] W. Schenk, H. Nabielek. *Testing of Irradiated Spherical Fuel Elements at HTR Modul Relevant Accident Condition*. Behavior of Gas Cooled Reactor Fuel under Accident Conditions. Proceedings of aSpecialist Meeting held in Oak Ridge, 5-8 November 1990. IWGCR-25, pp 87-98

[31] J. H. Venter, H. Nabielek. *Fuel: Performance Envelope of Modern HTR TRISO Fuel Report*. 3rd International Topical Meeting on High Temperature Reactor Technology, October 1-4, 2006, Johannesburg, South Africa.

[32] M. A Futterer *et.al*. *Irradiation of High Temperature Reactor Fuel Pebbles at VHTR Conditions in the HFR of Petten*. 2nd International Topical Meeting on High Temperature Reactor Technology, September 22-24 2004, Beijing, China.

[33] http://www.fz-juelich.de/zfr/reaktor-e.html

[34] K. N. Koscheev *et.al*. *Experimental Capabilities of IVV-2M Reactor and its Research Complex to Determine Workability of Coated Particles and Fuel Element of High Temperature Gas Cooled*

Reactors. The First Information Exchange Meeting on Survey on Basic Studies in the Field of High Temperature Engineering, Paris, France, 27-29 September ,1999

[35] IAEA TECDOC-978. *Fuel Performance and Fission Product Behaviour in Gas Cooled Reactors.*

[36] C. Tang *et.al*. *Fuel Irradiation of the First Batches Produced for the Chinese HTR-10*. Nuclear Engineering and Design 236 (2000) 107-113.

[37] C. Tang *et al*. *The Behaviour of the HTR-10 Fuel under Irradiation*. 2nd International Topical Meeting on High Temperature Reactor Technology, September 22-24 2004, Beijing, China.

[38] A. Verwimp *et al*. *Irradiation and Post Irradiation Capabilities at the SCK.CEN*. The First Information Exchange Meeting on Survey on Basic Studies in the Field of High Temperature Engineering, Paris, France, 27-29 September ,1999

[39] M. Grounes et.al. *Fuel R & D* at Studsvik. *Introduction and Experimental Facilities*. Nuclear Engineering and Design 168 (1997) 129 – 149.

[40] D. T Goodin, M. J. Kania and B.W. Pattone. *Experimental Plan for Irradiation Experiment HRB-21*. DOE-HTGR-87091 and ORNL/TM-10987.

[41] D. Petti, et.al. *Development of Improved Models and Designs for Coated Particle Gas Reactor Fuels*. Annual Progress Report Under the International Nuclear Energy Research Initiative (I-NERI)

[42] S. Bendotti, P. Guillermier, M.Phelip. *HTR and VHTR Fuel Irradiation Program in the OSIRIS Material Testing Reactor*. 2nd International Topical Meeting on High Temperature Reactor Technology. Beijing, China, September 22-24, 2004

[43] P. Guillermier, M. Phelip. *AREVA and CEA Fuel Development and Qualification of HTR Fuel*. HTR2006: 3rd International Topical Meeting on High Temperature Reactor Technology. October 1-4, 2006, Johannesburg, South Africa.

[44] A. Languille. *HTR Coated Particles and Fuel Elements Present Development*. HTR/ECS 2002. https://odin/jrc/nl/htr-tn/HTR-Eurocourse-2002/Languille_567.pdf

[45] G. Ball *et.al*. *Neutronic Study on Conversion of SAFARI-1 to LEU Silicide Fuel*. Proceedings of the 1994 International Meeting on Reduced Enrichment for research and Test Reactors, Williamsburg, 18-23 September, 1994

[46] A. Muller. *Establishment of the Technology to Manufacture Uranium Dioxide Kernels for PBMR Fuel*. HTR2006: 3rd International Topical Meeting on High Temperature Reactor Technology. Johannesburg, South Africa, October 1-4, 2006

[47] J. J. Duderstadt, L. J. Hamilton. *Nuclear Reactor Analysis*. 1976, John Wiley & Sons.

[48] W. M. Stacey. *Nuclear Reactor Physics*. 2001. John Wiley & Sons.

[49] F. Reitsma, W. R. Joubert. *A Calculational System to Aid Economical Use of the MTRs*. Research Reactor Fuel Management Conference (RRFM), Bruges, Belgium, 28 -30 March 1999

[50] T. Goorley. LANL X-5. *Criticality Calculations with MCNP5: A Primer*. 2nd edition. LA-UR-04-0294.

[51] J. R. Lamarsh, A. Baratta. *Introduction to Nuclear Engineering*. 3rd edition. Addison-Wesley series in Nuclear Science and Engineering.

[52] S. Glasstone, A. Sesonke. *Nuclear Reactor Engineering*. 3rd edition.

[53] T. V. Blosser and G. E. Thomas (Jr). *Neutron Flux and Neutron and Gamma-Ray Spectra Measurements at the HFIR*. ORNL-TM-2221, 24 June 1968

[54] E. Malášek. *Proceedings of an International Seminar on InterComparison of Reactor Calorimeters*. Poland, 15-27 May 1972

[55] M. Belal, *et.al*. *Analysis of the Calculational Techniques of Heat Deposition via MCNP in Comparison with a Calorimeter Experiment at the SAFARI-1 Research Reactor*. 12th Annual Research Reactor Fuel Management conference, Hamburg, Germany, 2-5 March 2008.